Article scientifique   Article   2019   Published version   Open Access

Increased cerebral blood volume in small arterial vessels is a correlate of amyloid-β-related cognitive decline
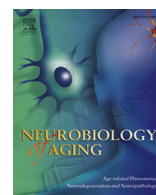
Hua, Jun; Lee, SeungWook; Blair, Nicholas I S; Wyss, Michael; van Bergen, Jiri M G; Schreiner, Simon J; Kagerer, Sonja M; Leh, Sandra E; Gietl, Anton F; Treyer, Valerie; Buck, Alfred; Nitsch, Roger M; Pruessmann, Klaas P; Lu, Hanzhang [**and 4 more**]

Increased cerebral blood volume in small arterial vessels is a correlate of amyloid-β–related cognitive decline

Check for updates

Jun Hua [a,b], SeungWook Lee [c], Nicholas I.S. Blair [c], Michael Wyss [d], Jiri M.G. van Bergen [e], Simon J. Schreiner [e,f], Sonja M. Kagerer [e,f], Sandra E. Leh [e], Anton F. Gietl [e], Valerie Treyer [e,g], Alfred Buck [g], Roger M. Nitsch [e], Klaas P. Pruessmann [d], Hanzhang Lu [a,b], Peter C.M. Van Zijl [a,b], Marilyn Albert [h], Christoph Hock [e], Paul G. Unschuld [e,f,*]

[a] Neurosection, Division of MRI Research, Department of Radiology, Johns Hopkins University School of Medicine, Baltimore, MD, USA
[b] F.M. Kirby Research Center for Functional Brain Imaging, Kennedy Krieger Institute, Baltimore, MD, USA
[c] Department of Biomedical Engineering, Johns Hopkins University, Baltimore, MD, USA
[d] Institute for Biomedical Engineering, University of Zurich and ETH Zurich, Zurich, Switzerland
[e] Institute for Regenerative Medicine (IREM), University of Zurich, Schlieren, Switzerland
[f] Hospital for Psychogeriatric Medicine, Psychiatric University Hospital Zurich (PUK), Zurich, Switzerland
[g] Department of Nuclear Medicine, University Hospital Zurich, Switzerland
[h] Department of Neurology, Johns Hopkins University School of Medicine, Baltimore, MD, USA

ARTICLE INFO

ABSTRACT

The protracted accumulation of amyloid-β (Aβ) is a major pathologic hallmark of Alzheimer's disease and may trigger secondary pathological processes that include neurovascular damage. This study was aimed at investigating long-term effects of Aβ burden on cerebral blood volume of arterioles and pial arteries (CBVa), possibly present before manifestation of dementia. Aβ burden was assessed by 11C Pittsburgh compound-B positron emission tomography in 22 controls and 18 persons with mild cognitive impairment (MCI), [ages: 75(±6) years]. After 2 years, inflow-based vascular space occupancy at ultra-high field strength of 7-Tesla was administered for measuring CBVa, and neuropsychological testing for cognitive decline. Crushing gradients were incorporated during MR-imaging to suppress signals from fast-flowing blood in large arteries, and thereby sensitize inflow-based vascular space occupancy to CBVa in pial arteries and arterioles. CBVa was significantly elevated in MCI compared to cognitively normal controls and regional CBVa related to local Aβ deposition. For both MCI and controls, Aβ burden and follow-up CBVa in several brain regions synergistically predicted cognitive decline over 2 years. Orbitofrontal CBVa was positively associated with apolipoprotein E e4 carrier status. Increased CBVa may reflect long-term effects of region-specific pathology associated with Aβ deposition. Additional studies are needed to clarify the role of the arteriolar system and the potential of CBVa as a biomarker for Aβ-related vascular downstream pathology.

© 2019 The Authors. Published by Elsevier Inc. This is an open access article under the CC BY license (http://creativecommons.org/licenses/by/4.0/).

1. Introduction

Late-onset Alzheimer's disease (AD) is characterized by a decade-long preclinical phase and eventually leads to mild cognitive impairment (MCI) as its first clinical manifestation (Albert et al., 2011). Although neuropathological changes in AD are complex and include cerebrovascular disease, neuroinflammation, and aggregation of pathological tau and other proteins (Elahi and Miller, 2017; Serrano-Pozo et al., 2011), Aβ-burden is considered to represent earliest brain pathology in AD and possibly trigger a multitude of pathologic downstream processes (Jack et al., 2010; Ossenkoppele et al., 2015; Rabinovici et al., 2017; Villemagne et al., 2018). The advent of positron emission tomography (PET) tracers such as 11C-Pittsburgh Compound B (PiB) has provided the means to non-invasively assess the extent of regional amyloid-β (Aβ) burden in older populations (Klunk et al., 2004; Seo et al., 2017; van Bergen et al., 2018b). By now, a concatenation of studies have

consistently demonstrated that the risk for cognitive decline and dementia is closely related to the cerebral accumulation of Aβ, as measured by PET, cerebrospinal fluid, or postmortem examination (Jansen et al., 2015; Mormino et al., 2009; Roberts et al., 2017). Moreover, progression of pathology in AD is linked to neurovascular dysfunction (Iadecola, 2004; Iturria-Medina et al., 2016), as reflected by reduced cerebral blood flow (CBF) and also altered blood-brain barrier permeability (Bell and Zlokovic, 2009; Kisler et al., 2017; Leeuwis et al., 2017; Ostergaard et al., 2013). The co-occurrence of AD-typical neurometabolic change and vascular pathology may support the idea of synergistic interaction of vascular change and neurodegeneration as an aggravating factor for pathology in AD (Gelber et al., 2012; Schreiner et al., 2018; Snowdon and Nun, 2003; Tyas et al., 2007a,b). Interestingly, apolipoprotein E e4 (APOE4), which is the strongest known genetic risk factor for AD (Corder et al., 1993; Verghese et al., 2013), is associated with accelerated accumulation of Aβ, reduced CBF, and impaired blood-brain barrier function (Janelidze et al., 2017; Thambisetty et al., 2010). Particularly, reduced brain perfusion (CBF) (Michels et al., 2016; Thambisetty et al., 2010) and impaired cerebrovascular reactivity (Suri et al., 2015) have been observed in cognitively normal APOE4 carriers. Therefore, it is important to assess the association between APOE4 and cerebrovascular impairments in AD. Although the accumulation of Aβ in sporadic AD is mainly caused by decreased clearance (Mawuenyega et al., 2010), clearance capacity of Aβ from the brain depends on interstitial spinal fluid flow in the paravascular space surrounding arterioles, which is primarily driven by the arterial pulsation wave from the small blood vessels (Iliff et al., 2012, 2013; Xie et al., 2013). This indicates that abnormalities in arterioles may contribute to accumulation and deposition of Aβ and possibly other toxic solutes related to neurodegenerative brain dysfunction. Cerebral blood volume (CBV) is a measure of the quantity of blood in a unit of tissue (Hua et al., 2018). Although CBV generally is linked to regional tissue metabolism, arteriolar CBV (CBVa) particularly reflects the autoregulatory capacity of arteriolar vessel resistance, and thus may be used to investigate cerebrovascular functionality within gray matter regions (Aaslid et al., 1989; Gröhn et al., 1998; Grubb et al., 1974; Petrella and Provenzale, 2000; Rane et al., 2016). CBVa may be assessed by inflow vascular space occupancy (iVASO) magnetic resonance imaging (MRI) (Donahue et al., 2010; Hua et al., 2011a), and application of ultrahigh field strength of 7 Tesla (7T) provides high signal-to-noise ratios (SNRs) (Hua et al., 2017; Wu et al., 2016). Recently, reductions in total CBV have been demonstrated in patients with AD dementia (Harris et al., 1996; Lacalle-Auterioles et al., 2014; Nielsen et al., 2017b; Uh et al., 2010). Based on these earlier findings, we hypothesized that CBVa may be a particularly sensitive indicator of AD-related gray matter (GM) pathology and thus reflect vascular downstream effects of Aβ in the predementia stage. To test this hypothesis, a nondemented study population comprising cognitive performance levels from normal to MCI, received 11C-PiB-PET for assessment of regional Aβ burden, and as a follow-up after 2 years, iVASO MRI at ultrahigh field strength of 7T. In addition, genetic risk for AD as indicated by APOE4 carrier status and cognitive decline within the study period were used as covariates.

2. Methods

2.1. Participant characteristics

We recruited 18 patients with MCI and 22 cognitively unimpaired older adults as controls. Patients with MCI and healthy controls were recruited as part of an ongoing study at our hospital, and matched by age and sex, as reported in detail earlier (Gietl et al., 2015; Schreiner et al., 2014, 2016; Steininger et al., 2014). Exclusion

criteria were any present medication that may affect cognition, general MRI exclusion criteria, contraindications against venipuncture, clinically relevant changes in red blood cell count, any acute severe medical, neurological, or psychiatric condition, present or past drug abuse, allergy to the PET tracer 11C-PiB, significant earlier exposure to radiation. The study was conducted in accordance with guidelines issued by the local ethics committee (Kantonale Ethikkommission Zurich) and with the declaration of Helsinki (World_Medical_Association, 1991). All procedures were approved by the Kantonale Ethikkommission Zurich. All participants gave written informed consent before scanning. Each participant had 2 visits approximately 2 years apart (730 ± 277 days) and received neuropsychological testing at both time points (TP1 and TP2). PET studies were performed at study inclusion; the 7 Tesla MR sequences were administered during the follow-up visit, resulting in an average delay of 803 ± 203 days between PET and 7T MRI measures. Demographic data and factors associated with vascular risk are summarized in Table 1. Isoforms of the APOE gene were assessed for all participants. Twelve of the participants carried 1 e4 allele and 2 participants carried 2 e4 alleles.

2.2. Neuropsychological testing

All participants received detailed clinical and neuropsychological examination before they were included in the present study. Participants were categorized either as cognitively normal or MCI according to established criteria (Albert et al., 2011). All participants were screened for cognitive impairment using the Mini-Mental State Examination (Folstein et al., 1975). Cognitive performance of study participants was assessed at TP1 and TP2 based on 4 cognitive tests: (1) The Revised Boston Naming Test (Nicholas et al., 1988); (2) Digit Spans Backward (Gregoire and Van der Linden, 1997); (3) Trail Making Test B/A (Tombaugh, 2004); and (4) Verbal Learning And Memory Test: delayed recall (Lange et al., 2002). These measures were z-score-transformed and averaged to generate a single global cognitive score for each participant. Longitudinal changes in the cognitive scores were normalized by the time duration (in years) between the 2 visits.

Table 1
Demographics and test performance of the study population

Variable	Controls[a]	Patients with MCI[a]	p Value[b]
N	22	18	N/A
Sex (female)	8	6	1
Age (y)	72 ± 5	75 ± 7	0.08
Education (y)	13.64 ± 2.56	15.06 ± 3.28	0.13
Number of APOE4 alleles	7	9	N/A
Body mass index (BMI)	25.24 ± 4.13	24.57 ± 3.83	0.60
Arterial hypertension (N: yes; no)	4; 18	8; 10	0.07
Hypercholesterinemia (N: yes; no)	4; 18	9; 9	0.03
Present smokers (N: yes; no)	1; 21	0; 18	1
History of past smoking (N: yes; no)	9; 13	10; 8	0.36
Mini-Mental State Examination (MMSE), % change per year	0.57 ± 3.6	−0.63 ± 5.04	0.4
Boston naming test (BNT), % change	−1.46 ± 4.46	0.19 ± 10.63	0.54
Digit span backward, % change	−1.35 ± 21.17	4.89 ± 26.83	0.42
Trail making B/A (TMT B/A), % change	4.11 ± 35.41	−9.21 ± 67.44	0.45
Verbal learning and memory (VLMT), % change	−8.43 ± 28.9	−31.49 ± 100.72	0.35
Cognitive performance score (Z), %SD change	−0.9 ± 37.45	−6.19 ± 71.54	0.77

[a] Mean ± standard deviation (SD).
[b] p values from 2-sample t-tests between the 2 groups, or from χ²-test for categorical variables. Neuropsychological scores indicate average % changes in test performance between study inclusion (TP1) and follow-up (TP2).

2.3. Magnetic resonance imaging

All scans were performed on a 7T Philips MRI scanner (Philips Healthcare, Best, The Netherlands). A 32-channel phased-array head coil (Nova Medical, Wilmington, MA) was used for radio-frequency reception and a head-only quadrature coil for transmit. High-resolution anatomical images were acquired with a 3D magnetization prepared 2 rapid acquisition gradient echoes (MP2RAGE) sequence (Marques et al., 2010; Van de Moortele et al., 2009) (voxel = 0.75 mm isotropic). Total scan time on the 7T instrument was 50:42 minutes, including 10:43 minutes for performing the MP2RAGE sequence and 8:19 minutes for obtaining iVASO data.

Three-dimensional iVASO MRI was performed to measure regional GM CBVa. In iVASO MRI, arterial and arteriolar blood signal is zeroed out (nulled) by applying a spatially selective inversion in regions containing major feeding arteries. The difference signal between the arterial blood nulled scan and a control scan without blood nulling can then be used to calculate CBVa (Donahue et al., 2010; Hua et al., 2011c, 2014; Wu et al., 2016). To account for the heterogeneity of vascular transit times, interleaved nulling and control images are acquired at multiple postinversion delay times (TI), and a biophysical model for multi-TI iVASO signals is used to numerically fit absolute CBVa from the dynamic multi-TI time course on a voxel-by-voxel basis so that the vascular transit time can be different in each voxel (Hua et al., 2011c). Crushing gradients can be incorporated to suppress signals from fast-flowing blood in large arteries and thereby sensitize this method to CBVa predominantly in the pial arteries and arterioles, which we refer to here as arteriolar blood. The iVASO approach was originally developed in a single-slice mode using a gradient echo echo planar imaging readout and has now been extended to a 3D sequence with whole-brain coverage (Hua et al., 2013, 2017). The following iVASO parameters were used: time of repetition/TI = 10000/1383, 5000/1093, 3800/884, 3100/714, 2500/533, and 2000/356 ms; 3D fast gradient echo readout (TE = 2.2 ms); voxel = $3.5 \times 3.5 \times 5$ mm^3, 20 slices; parallel imaging acceleration (SENSE) = 2×2; crusher gradients of b = 0.3 s/mm^2. A reference scan (time of repetition = 20 seconds, other parameters identical) was obtained to determine the scaling factor M0 in iVASO images so that absolute CBVa values can be calculated.

2.4. MRI data analysis

The statistical parametric mapping (SPM) software package (version 8, Wellcome Trust Centre for Neuroimaging, London, United Kingdom; http://www.fil.ion.ucl.ac.uk/spm/) and other in-house code programmed in MATLAB (MathWorks, Natick, MA, USA) were used for image analysis. iVASO images were motion-corrected using the realignment routine in SPM. As the nulling and control scans in iVASO are acquired in an interleaved order and the MR signal difference between nulling and control images is usually less than 1%—3% of the total signal (because it reflects the arteriolar blood volume in the voxel) (Hua et al., 2011c), we aligned all nulling and control images to the first control image acquired in the series. Anatomical images were coregistered with iVASO images and normalized to the Montreal Neurological Institute (MNI) space using SPM. GM, white matter (WM), and cerebrospinal fluid (CSF) maps were generated from the anatomical images using the SPM segmentation algorithm. No spatial smoothing was performed in the analysis. The surround subtraction method (Lu et al., 2006) was used to calculate the difference signal from the nulling and control iVASO images. Partial volume effects of WM and CSF on the iVASO difference signal in GM were corrected (Johnson et al., 2005) (results without partial volume correction are also reported). An SNR

threshold of one standard deviation below the mean SNR was used to exclude voxels with insufficient SNR from further analysis (Hua et al., 2011c). In our data, about 10% of voxels were excluded, most of which are close to the skull and the sinus regions. This SNR threshold was applied on each subject's data. If a voxel falls below the threshold in one subject, it will be excluded from all subjects in the group analysis. In our data, most of these voxels overlapped in multiple subjects. Whole-brain GM CBVa maps were numerically fitted from the iVASO difference signals at all TIs with the iVASO equations (Hua et al., 2011c) using in-house MATLAB code.

2.5. PiB—positron emission tomography

PiB-PET was used to estimate individual brain Aβ plaque load as described in earlier publications (Quevenco et al., 2017; van Bergen et al., 2016). In brief, an individual dose of approximately 350 MBq of carbon-labeled PiB was injected into the cubital vein. A standard quantitative filtered back projection algorithm including necessary corrections was applied. Cortical late frame (minutes 50—70) values were divided by the cerebellar GM average, resulting in PiB-PET relative standard uptake values (SUVr; matrix = $128 \times 128 \times 47$, voxel size = $2.3 \times 2.3 \times 3.3$ mm^3). Measures of individual regional brain Aβ load were derived from the ratio of regional PiB-SUV, referenced to cerebellar SUV, after coregistration of PET images to the 7T MP2RAGE volumes using SPM 12 software.

2.6. Statistics

Group differences in GM CBVa maps were examined using analysis of variance with age, sex, education, regional GM volume from anatomical scans and motion parameters estimated from the motion correction (realignment) routine in SPM accounted for as covariates in the analysis. Significant clusters of increased or decreased GM CBVa were identified using in-house MATLAB code implemented using the threshold-free cluster enhancement method (Smith and Nichols, 2009). Briefly, permutation testing was conducted by testing the threshold-free cluster enhancement output against the null distribution across permutations and obtaining the 95th percentile in the null distribution as the corrected $p < 0.05$ level. The IBASPM 116 atlas (Lancaster et al., 1997, 2000; Maldjian et al., 2003, 2004; Tzourio-Mazoyer et al., 2002) (PickAtlas software, Wake Forest University, North Carolina, USA) was used to identify anatomical regions within the significant clusters. Effect size was estimated with Cohen's d. Correlations between CBVa values and Aβ (PiB ratio) in each region, as well as APOE4 carrier status were evaluated using data combined from all participants (including both MCI and controls). Partial correlations were calculated with age, sex, and education as covariates. All statistical tests were corrected for multiple comparisons by controlling the false discovery rate (adjusted $p < 0.05$) (Benjamini and Hochberg, 1995). Multiple regression was carried out using MATLAB to test the potential synergistic effects from GM CBVa and Aβ (reflected in the β3 term in the following equation) on longitudinal cognitive decline using the following model:

$$
\begin{aligned}
\text{Cognitive decline (\% per year)} = {} & \beta 0 + \beta 1 \times \text{CBVa} + \beta 2 \times \text{A}\beta \\
& + \beta 3 \times \text{CBVa} \times \text{A}\beta + \beta 4 \\
& \times \text{sex} + \beta 5 \times \text{age} + \beta 6 \\
& \times \text{education} + \beta 7 \times \text{age} \\
& \times \text{A}\beta
\end{aligned}
$$

In addition, multilevel regression analysis using data from the control and MRI subjects as 2 separate groups was also performed.

3. Results

As shown in Table 1, age, sex, and education levels were matched between patients with MCI and controls ($p > 0.1$). No significant differences were found in motion parameters derived from the SPM realignment routine between the 2 groups. Performance in the Verbal Learning And Memory Test and Mini-Mental State Examination tests differed between controls and MCI both at study inclusion (TP1) and follow-up (TP2) (Supplement 3, Table 9, Fig. S2). Although there was considerable variability in % changes of performance from TP1 to TP2 on an individual level (Table 1), no significant changes between TP1 and TP2 resulted for any of the investigated tests on a group level (Table 9, Fig. S2). None of the participants progressed to AD dementia from TP1 to TP2. Participants of the MCI group had a higher prevalence of hypercholesterinemia and a trend for higher prevalence of arterial hypertension (Table 1). An individual subject level iVASO CBVa map from one control subject is shown in Fig. 1 to demonstrate typical data quality.

Tables 2 and 3 summarizes the main findings in the group comparisons. The average GM CBVa values in controls were all in normal range (Hua et al., 2011c, 2018), providing validation for our measurements. Widespread elevation of GM CBVa was detected in many brain regions in patients with MCI compared with controls with relative changes of 17.0%–122.0% and effect sizes of 0.75–1.56. Most of these changes were detected in both hemispheres in corresponding regions, although the cluster sizes varied between the left and right hemispheres in some regions. Significant reduction of GM CBVa was also observed in a few brain regions, but the spatial extent was much smaller than increased CBVa. Some brain regions showed both decreased and increased GM CBVa values in different subregions. No significant difference was found in mean GM CBVa over the whole brain (including all GM voxels, not just significant clusters) between patients and controls. The partial volume correction procedure did not seem to have a major effect on the measured CBVa values (Table 3). Fig. 2A displays the regions with significant increased or decreased GM CBVa in patients with MCI on MNI normalized anatomical images, with an intensity reflecting the relative changes in each significant voxel. Fig. 2B shows the areas with significantly increased PiB-PET retention in patients with MCI on MNI normalized anatomical images.

From the correlation analysis, many regions with increased CBVa values colocalized with regions with increased Aβ deposition, with significant positive correlations between the 2 in several brain regions (Table 4, Fig. 2C). Scatter plots from 2 of these regions are shown in Fig. 3. In most of these regions, synergistic effects from GM CBVa and Aβ on longitudinal cognitive decline were found using multiple regression (Tables 5 and 6 and Fig. S1). In regions with only significant CBVa or Aβ changes, no such synergistic effects were found. In addition, GM CBVa in 2 subregions in the orbitofrontal cortex also showed significant positive correlation with APOE4 carrier status (Supplement 1, Table 7, Fig. 3). Here, by applying multiple regression analysis, synergistic effects from GM CBVa and APOE4 on cognitive decline in multiple brain regions were found (Supplement 2, Table 8). Sex, age, and education were included as covariates in the correlation analysis.

4. Discussion

By applying ultrahigh field strength MRI at 7T to a study population of nondemented older adults, significantly elevated CBVa in patients with MCI could be observed. Interestingly, for the entire study population, an association between high local deposition of Aβ, as measured by 11C-PiB-PET, and elevated CBVa, as measured by iVASO at 7T 2 years later, was observable in many brain regions. Moreover, Aβ burden and CBVa at follow-up in several brain regions synergistically predicted cognitive performance over 2 years, when applying a linear regression model. Consistently, CBVa in the orbitofrontal cortex also showed a synergistic interaction with APOE4 carrier status regarding its relationship to cognitive change.

For this study, ultrahigh field strength MRI at 7T was used to acquire MP2RAGE structural images and 3D iVASO data for measuring whole-brain absolute CBVa maps (Donahue et al., 2010; Hua et al., 2011c, 2014, 2017; Marques et al., 2010; Van de Moortele et al., 2009; Wu et al., 2016). The combination of these technologies allows for high-resolution assessment of the homeostasis of pial arteries and arterioles in fine brain regions (Hua et al., 2018). Regional distribution of Aβ was investigated by 11C-PiB-PET as used by many earlier studies to investigate disease burden in preclinical and clinical stages of sporadic AD (Jansen et al., 2015; Klunk et al., 2004). The significantly higher burden of Aβ and its distribution pattern in the MCI group are consistent with earlier reports on pathological change in the predementia stage of AD (Jansen et al., 2015; Klunk et al., 2004; Roberts et al., 2017). Information on regional Aβ was complemented by assessment of the APOE4 genotype, which is the strongest known genetic risk factor for sporadic AD (Corder et al., 1993; Kantarci et al., 2012; Strittmatter et al., 1993). As a general indicator of cognitive performance in the study population, 4 German language versions of neuropsychological tests were performed to generate a composite score that integrates episodic memory, language, working memory, and executive function, as a representation of major domains affected early in AD (Albert et al., 2011). Our finding of lower test scores at follow-up in some study participants within the control group may reflect subtle cognitive changes associated with normal aging (Harada et al., 2013) or alternatively could be caused by nonspecific variation within the high-performance range of the used tests.

To our knowledge, this is the first report of microvascular abnormalities specifically in pial arteries and arterioles in GM (measured with CBVa) in an elderly, nondemented population at risk for AD. Although reductions in CBV and CBF have been reported earlier for AD dementia (Harris et al., 1996; Hauser et al., 2013; Lacalle-Aurioles et al., 2014; Nielsen et al., 2017b; Uh et al., 2010), investigations of neurovascular dysfunction in early, prodromal disease stages so far mainly have been focused on total CBV and CBF, which include arteriolar, capillary, and venular vessels (Gietl et al., 2015; Kisler et al., 2017; Leeuwis et al., 2017). Here, our findings of increased CBVa in older patients with MCI may be consistent with earlier reports suggesting an interaction of microvascular abnormalities and neurodegenerative pathology in AD (Iadecola and
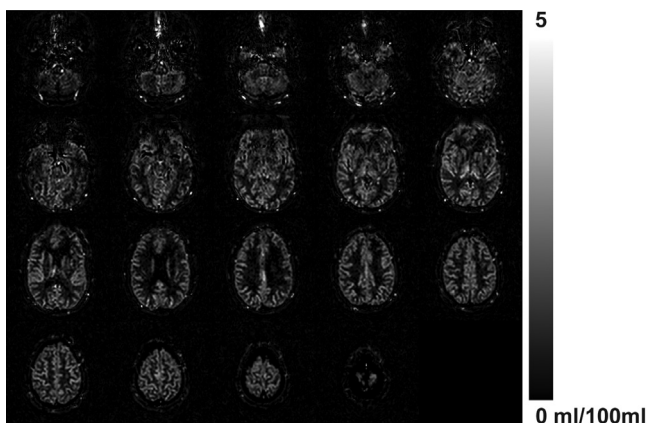

Fig. 1. Individual subject level CBVa map obtained using iVASO MRI in one control subject. Abbreviations: CBVa, arteriolar cerebral blood volume; iVASO, inflow-based vascular space occupancy; MRI, magnetic resonance imaging.

Table 2
GM CBVa in patients with MCI compared with controls in various brain regions

Region[a]	Hemisphere	Cluster size[b]	Cluster peak[c] (mm, MNI)			CBVa (mL blood/100 mL tissue)				Relative change (%)[d]	Effect size[e]	Adjusted p value
						MCI		Control				
			x	y	z	Mean	std	Mean	std			
Frontal_Sup_Orb	R	89	22	16	−14	2.75	1.88	1.32	1.11	108.2	1.00	0.015
Frontal_Sup_Orb	L	86	−18	22	−14	1.85	1.28	1.01	0.93	82.1	0.79	0.042
Frontal_Inf_Oper	R	239	54	12	14	1.54	0.43	1.08	0.25	41.8	1.40	0.049
Frontal_Inf_Oper	L	372	−46	14	2	1.34	0.28	1.09	0.14	23.7	1.26	0.004
Frontal_Inf_Tri	R	498	52	22	24	2.27	1.62	1.25	0.99	81.3	0.82	0.042
Frontal_Inf_Tri	L	752	−56	22	2	1.90	0.79	1.27	0.52	49.5	1.01	0.013
Frontal_Inf_Orb	R	557	32	30	−8	2.65	1.63	1.19	0.82	122.0	1.23	0.005
Frontal_Inf_Orb	L	200	−48	20	−8	2.15	1.44	1.07	0.99	100.8	0.93	0.019
Frontal_Sup_Medial	R	504	4	42	36	2.44	1.24	1.31	0.91	86.1	1.10	0.050
Frontal_Sup_Medial	L	390	−12	48	14	2.13	1.14	1.20	0.75	78.3	1.04	0.048
Frontal_Mid_Orb	R	346	2	22	−12	1.85	1.04	1.12	0.60	65.3	0.93	0.018
Frontal_Mid_Orb	L	178	−6	38	−8	1.89	0.91	1.27	0.67	49.1	0.82	0.028
Rolandic_Oper	R	265	40	−28	18	1.70	0.65	1.21	0.36	40.2	1.02	0.050
Rolandic_Oper	L	417	−54	−2	4	1.63	0.52	1.23	0.20	33.1	1.15	0.010
Supp_Motor_Area	R	136	2	−4	54	1.20	0.26	0.99	0.12	21.3	1.17	0.008
Supp_Motor_Area	L	78	0	−6	56	1.22	0.31	1.00	0.18	22.2	0.94	0.022
Olfactory	R	161	4	14	−14	2.31	1.19	1.13	0.81	103.9	1.24	0.003
Olfactory	L	146	−4	20	−14	2.06	1.11	1.08	0.80	90.1	1.07	0.008
Rectus	R	81	10	18	−14	2.46	1.17	1.16	1.01	111.4	1.24	0.002
Rectus	L	59	−8	22	−12	2.16	1.17	1.11	0.86	94.7	1.09	0.007
Insula	R	979	36	18	−12	2.39	1.13	1.23	0.69	93.5	1.33	0.002
Insula	L	761	−36	24	8	2.25	1.30	1.33	0.78	69.6	0.93	0.022
Cingulum_Ant	R	311	12	36	−8	2.16	1.12	1.29	0.94	66.8	0.88	0.029
Cingulum_Ant	L	504	−8	34	18	2.22	1.13	1.32	0.81	67.9	0.97	0.022
Cingulum_Mid	R	499	6	−8	44	1.21	0.16	1.04	0.07	17.0	1.56	0.001
Cingulum_Mid	L	338	−4	−2	40	1.30	0.23	1.08	0.11	20.3	1.35	0.003
Hippocampus	R	56	28	−36	8	1.78	0.93	1.05	0.57	69.2	1.01	0.014
Hippocampus	L	84	−22	−26	−12	1.76	0.84	1.08	0.65	63.9	0.96	0.013
Lingual	R	35	22	−50	2	2.35	0.88	1.79	0.69	31.4	0.75	0.047
Lingual	L	47	−22	−56	−4	1.37	0.47	1.08	0.15	26.9	0.94	0.035
Caudate	R	209	14	10	−12	2.34	1.65	1.16	1.17	101.4	0.88	0.026
Caudate	L	178	−10	18	−10	2.26	1.61	1.17	1.31	93.3	0.78	0.039
Putamen	R	422	24	22	−8	1.93	1.25	1.06	0.79	82.7	0.90	0.025
Putamen	L	441	−28	−2	−4	2.40	1.38	1.51	1.01	58.7	0.78	0.044
Temporal_Sup	R	518	54	0	−14	1.88	0.86	1.25	0.50	50.2	0.97	0.019
Temporal_Sup	L	955	−56	4	−2	1.83	0.91	1.17	0.36	56.3	1.05	0.017
Temporal_Pole_Sup	R	272	50	14	−12	2.46	1.33	1.30	0.76	88.5	1.16	0.006
Temporal_Pole_Sup	L	205	−58	6	−4	2.00	1.20	1.01	0.64	98.1	1.12	0.009

Key: CBVa, arteriolar cerebral blood volume; GM, gray matter; MCI, mild cognitive impairment; MNI, Montreal Neurological Institute; std, standard deviation.

[a] The brain regions were labeled according to the IBASPM 116 atlas (please see Methods for references).
[b] Number of voxels that shows significant group difference in this region.
[c] Location of the voxel with the maximum (peak) T-score in the cluster in the MNI space.
[d] Relative change was defined as 100 * (mean CBVa in MCI−mean CBVa in controls)/(mean CBVa in controls) %.
[e] Effect size was estimated with Cohen's $d = $ (mean CBVa in MCI−mean CBVa in controls)/s, where s is the pooled standard deviation of the 2 groups.

Nedergaard, 2007; Kisler et al., 2017; Schreiner et al., 2018). The close relationship between CBVa changes and local Aβ deposits in our data is in agreement with earlier considerations of consecutive vascular damage, impaired cerebrovascular autoregulation, and effects attributable to Aβ toxicity (Brickman et al., 2015; Zlokovic, 2011). In addition, our finding of a significant interactive effect of CBVa and Aβ in several brain regions on cognitive performance over 2 years, as measured by linear regression analysis, corroborates the relevance of vascular change for functional decline due to AD pathology (Helzner et al., 2009). Such interactive effect was not found in regions without overlapping CBVa or Aβ changes. Concordantly, we also find a synergistic effect of CBVa and APOE4 on cognitive performance over time, which may indicate relevance of increased CBVa regarding the individual risk to develop AD dementia. Our observation of a relationship between increased CBVa with Aβ and also APOE4 may reflect impaired cerebrovascular regulation, possibly caused by a direct impact of toxic Aβ aggregates on cerebral vessel walls (Kisler et al., 2017). Considering reports on a significant role of interstitial bulk flow for clearance of Aβ and other neurodegenerative proteins from the central nervous system that involves bidirectional CSF movement through paravascular spaces of pial arteries (Iliff et al., 2012), further preclinical studies are needed to investigate whether vasodilatation and thus increased CBVa might be caused by direct toxic impact of Aβ. Considering pathological changes of CBVa as a potential consequence of initial Aβ toxicity, iVASO might represent a marker of secondary cerebrovascular "downstream" pathology, as demanded recently for prospective clinical trials that allow for comorbid pathology in AD (Rabinovici et al., 2017). Alternatively, impaired arterial pulsation might reduce paravascular drainage of Aβ and as such could be consistent with the notion of a relationship between deteriorated microvascular hemodynamics and buildup of AD pathology (Iadecola, 2003; Nielsen et al., 2017b). Moreover, our observation of an association between APOE4, increased CBVa, and cognitive decline might also confirm earlier reports of APOE4 as a modulator of harmful Aβ effects on cognitive function (Kantarci et al., 2012). Consistently, brain regions with significant correlations between CBVa and Aβ in our study included the neocortex and hippocampal formation, which are considered particularly susceptible for AD pathology (Murray et al., 2015).

Table 3
GM CBVa in patients with MCI compared with controls in various brain regions (without partial volume correction)

Region[a]	Hemisphere	Cluster size[b]	Cluster peak[c] (mm, MNI)			CBVa (mL blood/100 mL tissue)				Relative change (%)[d]	Effect size[e]	Adjusted *p* value
						MCI		Control				
			x	y	z	Mean	std	Mean	std			
Frontal_Sup_Orb	R	89	22	16	−14	2.48	1.70	1.22	1.02	104.1	0.98	0.020
Frontal_Sup_Orb	L	86	−18	22	−14	1.67	1.16	0.93	0.86	78.5	0.76	0.046
Frontal_Inf_Oper	R	239	54	12	14	1.36	0.38	0.97	0.22	40.3	1.36	0.050
Frontal_Inf_Oper	L	372	−46	14	2	1.21	0.25	0.98	0.13	22.8	1.22	0.005
Frontal_Inf_Tri	R	498	52	22	24	2.04	1.46	1.13	0.89	80.6	0.81	0.043
Frontal_Inf_Tri	L	752	−56	22	2	1.68	0.70	1.17	0.48	43.9	0.92	0.016
Frontal_Inf_Orb	R	557	32	30	−8	2.34	1.44	1.08	0.75	116.0	1.19	0.006
Frontal_Inf_Orb	L	200	−48	20	−8	1.92	1.29	0.99	0.91	94.9	0.89	0.023
Frontal_Sup_Medial	R	504	4	42	36	2.22	1.13	1.18	0.82	87.9	1.12	0.051
Frontal_Sup_Medial	L	390	−12	48	14	1.90	1.02	1.08	0.68	75.7	1.01	0.051
Frontal_Mid_Orb	R	346	2	22	−12	1.66	0.93	1.01	0.54	65.0	0.93	0.020
Frontal_Mid_Orb	L	178	−6	38	−8	1.68	0.81	1.14	0.61	47.1	0.80	0.032
Rolandic_Oper	R	265	40	−28	18	1.54	0.58	1.12	0.33	37.4	0.96	0.054
Rolandic_Oper	L	417	−54	−2	4	1.45	0.46	1.12	0.19	29.5	1.04	0.015
Supp_Motor_Area	R	136	2	−4	54	1.08	0.23	0.91	0.11	19.1	1.07	0.012
Supp_Motor_Area	L	78	0	−6	56	1.10	0.28	0.90	0.16	22.5	0.95	0.023
Olfactory	R	161	4	14	−14	2.10	1.08	1.04	0.75	100.9	1.21	0.006
Olfactory	L	146	−4	20	−14	1.87	1.01	0.99	0.73	89.1	1.06	0.009
Rectus	R	81	10	18	−14	2.20	1.05	1.05	0.92	109.3	1.22	0.002
Rectus	L	59	−8	22	−12	1.91	1.03	1.01	0.78	89.1	1.04	0.010
Insula	R	979	36	18	−12	2.11	1.00	1.12	0.63	88.7	1.28	0.004
Insula	L	761	−36	24	8	2.00	1.16	1.19	0.70	67.8	0.92	0.025
Cingulum_Ant	R	311	12	36	−8	1.95	1.02	1.17	0.85	67.4	0.88	0.033
Cingulum_Ant	L	504	−8	34	18	1.97	1.00	1.19	0.72	65.8	0.95	0.025
Cingulum_Mid	R	499	6	−8	44	1.10	0.15	0.93	0.06	17.5	1.60	0.004
Cingulum_Mid	L	338	−4	−2	40	1.16	0.20	0.98	0.10	18.3	1.23	0.007
Hippocampus	R	56	28	−36	8	1.61	0.85	0.95	0.52	69.2	1.01	0.018
Hippocampus	L	84	−22	−26	−12	1.57	0.75	0.96	0.58	62.8	0.95	0.016
Lingual	R	35	22	−50	2	2.09	0.78	1.65	0.63	26.3	0.64	0.048
Lingual	L	47	−22	−56	−4	1.22	0.42	1.00	0.13	22.0	0.79	0.036
Caudate	R	209	14	10	−12	2.10	1.48	1.06	1.07	98.9	0.86	0.030
Caudate	L	178	−10	18	−10	2.02	1.44	1.06	1.19	90.0	0.76	0.039
Putamen	R	422	24	22	−8	1.72	1.11	0.96	0.71	79.8	0.88	0.027
Putamen	L	441	−28	−2	−4	2.17	1.25	1.39	0.93	55.8	0.75	0.045
Temporal_Sup	R	518	54	0	−14	1.69	0.77	1.14	0.46	48.8	0.94	0.024
Temporal_Sup	L	955	−56	4	−2	1.64	0.82	1.05	0.33	56.0	1.05	0.020
Temporal_Pole_Sup	R	272	50	14	−12	2.23	1.21	1.20	0.70	86.3	1.14	0.009
Temporal_Pole_Sup	L	205	−58	6	−4	1.78	1.07	0.92	0.58	94.1	1.09	0.011

Key: CBVa, arteriolar cerebral blood volume; GM, gray matter; MCI, mild cognitive impairment; MNI, Montreal Neurological Institute; std, standard deviation.
[a] The brain regions were labeled according to the IBASPM 116 atlas (please see Methods for references).
[b] Number of voxels that show significant group difference in this region.
[c] Location of the voxel with the maximum (peak) T-score in the cluster in the MNI space.
[d] Relative change was defined as 100 * (mean CBVa in MCI−mean CBVa in controls)/(mean CBVa in controls) %.
[e] Effect size was estimated with Cohen's d = (mean CBVa in MCI−mean CBVa in controls)/s, where s is the pooled standard deviation of the 2 groups.

The significant CBVa increase observed here may appear contradictory with the well-established finding of reduced regional CBF in MCI (Alsop et al., 2010; Dvorak et al., 1999; Hirao et al., 2005; Roher et al., 2011; Ruitenberg et al., 2005; Thomas et al., 2015). Aβ has long been known as a powerful vasoconstrictor (Niwa et al., 2001). However, we think that our increased CBVa finding may be congruent with CBF reduction for the reasons explained subsequently. Note that CBV measured by MRI reflects the fractional volume of all blood vessels in a given voxel (i.e., the unit of CBV: mL blood per 100 mL tissue). Therefore, CBV is proportional to the cross-sectional vessel diameter, length of blood vessels, and overall number of blood vessels in the voxel. A decrease in cross-sectional vessel diameter often leads to a decrease in CBF (vasoconstriction). However, if the vessel density in the voxel increases (thus increased number of vessels) possibly due to angiogenesis or others, the overall CBV measured in the voxel can be increased. Indeed, recent studies in tau-overexpressing mice showed increased blood vessel volume (increased CBV) but reduced blood vessel diameter (reduced CBF) compared with controls (Bennett et al., 2018). In the cortex of these mice, overall blood vessel density was increased

compared with controls even when the cortical atrophy is accounted for and blood flow was altered and at times obstructed in some vessels. A qPCR assay revealed that several genes related to hypoxia and angiogenesis were increased more than 2 fold in these mice. Although these results were obtained in tau-overexpressing mice (rather than amyloid-based models), they indicate a possible explanation for the concomitant CBVa increase and CBF reduction. Besides, the uncoupling of CBF and CBV is often seen in circumstances in which there is increased metabolic demand or hypoxia and angiogenesis (Mishra, 2016; Puro et al., 2016); for instance, in ischemia, the pial arteries and arterioles are typically dilated to compensate for a lack of blood flow, so a situation of reduced CBF, with increased CBVa. Another possibility is elevated microvascular tortuosity (Thore et al., 2007), thus increased length of blood vessels. These hypotheses should be validated in future studies possibly combining MRI with other imaging techniques such as optical imaging. Second, as CBVa represents arteriolar fractions of total CBV (sum of arteriolar, capillary, and venular CBV), a distinct increase of CBVa might indicate a shift of volumes within the cerebrovascular system. Different types of blood vessels have distinct
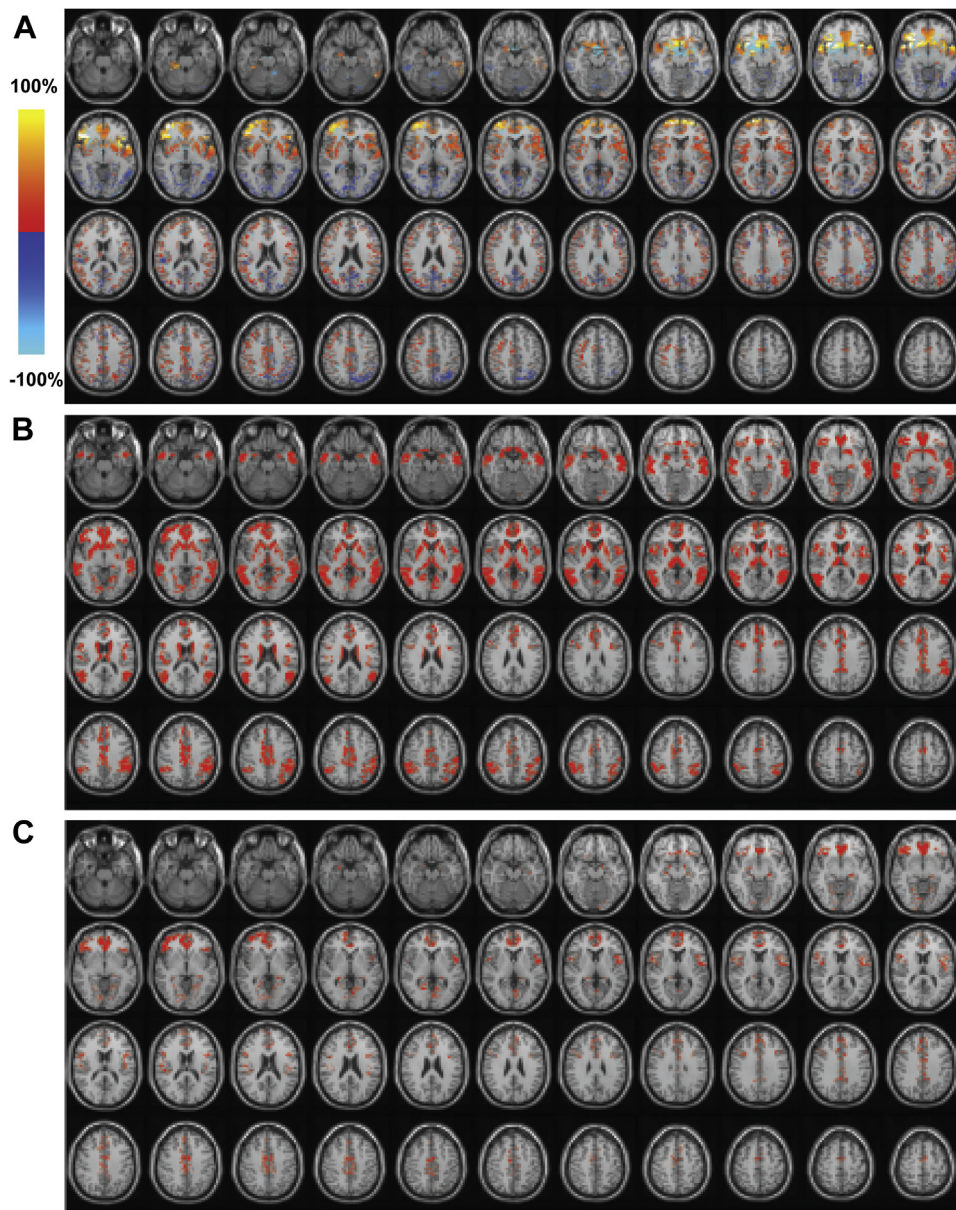
Fig. 2. (A) Map of relative CBVa changes between patients with MCI and controls overlaid on MNI normalized anatomical images. The relative change is defined as (100 × [MCI−control]/control)%. Only voxels that show significant CBVa difference between the 2 groups (adjusted $p < 0.05$) are highlighted. (B) Brain regions with abnormal PiB-PET retention overlaid on MNI normalized anatomical images. Only voxels that show significant PiB-PET difference between patients with MCI and controls (adjusted $p < 0.05$) are highlighted. (C) Colocalization of GM CBVa abnormality and β-amyloid deposit. Voxels that show significant correlation between GM CBVa values and PiB ratios are highlighted overlaid on MNI normalized anatomical images. Abbreviations: CBVa, arteriolar cerebral blood volume; GM, gray matter; MCI, mild cognitive impairment; MNI, Montreal Neurological Institute; MRI, magnetic resonance imaging; PiB-PET, 11C Pittsburgh compound-B positron emission tomography.

functions and physiology and can be affected differentially by the AD pathology. The arterioles are the most actively regulated blood vessels and thus may be more sensitive to metabolic disturbances in the brain (Iadecola and Nedergaard, 2007; Ito et al., 2001, 2005; Kim et al., 2007; Takano et al., 2006). For instance, significant reduction in CBVa has been observed in patients with schizophrenia (Hua et al., 2015, 2017), whereas no substantial changes in capillaries were indicated in histopathological studies in schizophrenia (Kreczmanski et al., 2005, 2009; Uranova et al., 2010). It should be noted that small diameter (<150 microns) pial arteries and arterioles (CBVa) only represents 10%–20% of total CBV (Hua et al., 2018; Piechnik et al., 2008; Sharan et al., 1989; van Zijl et al., 1998) (depending on vessel diameter), thus an 100% increase in CBVa would only translate to 10%–20% in total CBV change, which is

within the typical physiological range. The fact that CBVa values in controls were all within the normal range (Hua et al., 2018) and that CBVa in the cerebellum (which is not expected to be affected at this stage) did not show group differences also provides some validation for our results. Further studies are needed to investigate whether increase of CBVa in AD risk populations might possibly result in reduced total CBV in clinically manifest AD, as reported earlier (Eskildsen et al., 2017; Hauser et al., 2013; Lacalle-Aurioles et al., 2014; Nielsen et al., 2017b; Yoshiura et al., 2009). It is also worth noting that the synergetic effects between CBVa and other parameters were restricted to several small brain regions, which might be in agreement with the recent observation of regional AD-like biomarker patterns in at-risk populations (Wirth et al., 2017). Moreover, in our study, higher prevalence of hyperlipidemia were

Table 4
Correlation between GM CBVa and β-amyloid in multiple brain regions in all participants

Region[a]	Estimate coefficient	Standard error	p-Value
Frontal_Sup_Orb	2.32	0.38	<0.001
Frontal_Inf_Oper	0.31	0.14	0.006
Frontal_Inf_Orb	4.69	2.36	0.01
Frontal_Sup_Medial	3.33	1.32	0.006
Frontal_Mid_Orb	1.16	0.23	<0.001
Rolandic_Oper	0.67	0.26	0.001
Supp_Motor_Area	0.17	0.10	0.05
Cingulum_Ant	2.64	1.36	0.01
Cingulum_Mid	0.23	0.06	<0.001
Hippocampus	4.49	2.46	0.03
Lingual	1.70	0.86	0.01

Key: CBVa, CBVa, arteriolar cerebral blood volume; GM, gray matter.
[a] The brain regions were labeled according to the IBASPM 116 atlas (please see Methods for references).

observable for the MCI group, which may be consistent with earlier reports on an association between serum hypercholesterolemia and increased risk for the development of AD amyloid pathology (Pappolla et al., 2003).

It is important to discuss methodological factors for iVASO MRI, which might interact with MCI pathology to bias the study results. First, the presence of amyloid may introduce additional susceptibility effects at high field that can affect MR signals. Fortunately, in iVASO, CBVa is calculated from the difference signal between the arteriolar blood nulled image and the subsequent control image. Therefore, all static signals that are not flowing such as GM and WM should cancel out on subtraction (Hua et al., 2011b). Second, differences in cortical thickness among groups or over time may lead to different partial volume effects in the CBVa results. As this is an important confounding factor especially in this population in which substantial brain atrophy is expected, we corrected such partial volume effects in our analysis using a previously published method (Johnson et al., 2005) (see Methods Section). In addition, GM volume derived from anatomical images was included as a covariate in all statistical analyses to account for any residual partial volume effects. As shown in the Results Section, all major findings were consistent with and without the partial volume correction step. It is important to realize that iVASO MRI does not measure CBV in the capillaries (Hua et al., 2018) but only in the arterial compartment. This predominant arterial origin of the iVASO signal was validated
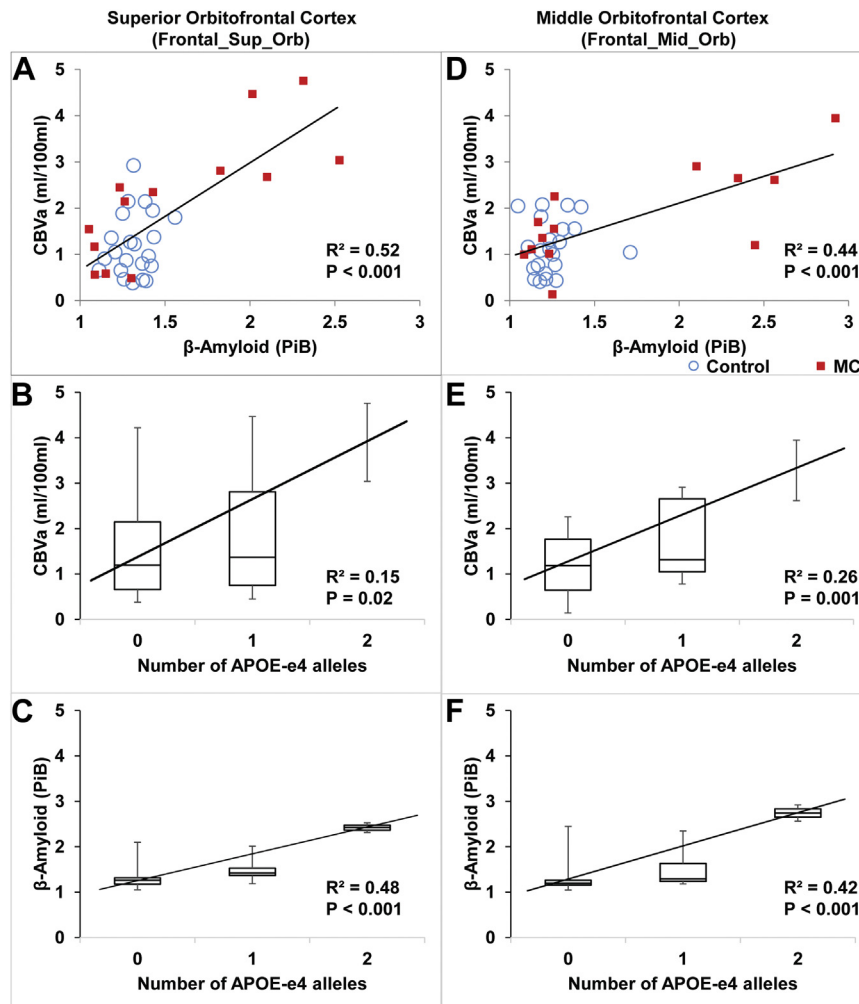

Fig. 3. Scatter plots show correlations between CBVa and β-amyloid, and boxplots show associations between CBVa, the number of APOE-e4 alleles, and between β-amyloid and the number of APOE-e4 alleles in the superior orbitofrontal cortex (Frontal_Sup_Orb, A-C) and the middle orbitofrontal cortex (Frontal_Mid_Orb, D-F), respectively. These 2 regions showed significant correlations between CBVa and both β-amyloid (Table 4) and number of APOE-e4 alleles (Supplement 1, Table 7). Several additional regions showed significant correlation between CBVa and β-amyloid (Table 4) but not between CBVa and number of APOE-e4 alleles. The trend lines and adjusted R^2 and P were obtained from linear regression using data combined from all participants. Abbreviations: APOE-e4, apolipoprotein E e4; CBVa, arteriolar cerebral blood volume; MCI, mild cognitive impairment; PiB, 11C Pittsburgh compound-B.

Table 5
Multiple regression shows synergistic effects from GM CBVa and β-amyloid on cognitive decline in multiple brain regions

Region[a]	Standardized coefficient[b,c]			p-Value			R²
	CBVa (β1)	Aβ (β2)	CBVa × Aβ (β3)	CBVa (β1)	Aβ (β2)	CBVa × Aβ (β3)	
Frontal_Sup_Orb							
Model 1[d] (full)	−1.47	−0.62	−1.77	0.05	0.05	0.05	0.31
Model 2[e] (restricted)		−0.27			0.05		0.15
F-test (p)[f]							0.05
Frontal_Inf_Orb							
Model 1[d] (full)	−1.46	−1.02	−1.76	0.05	0.03	0.05	0.39
Model 2[e] (restricted)		−0.51			0.05		0.16
F-test (p)[f]							0.01
Frontal_Sup_Medial							
Model 1[d] (full)	−1.52	−0.97	−2.14	0.02	0.02	0.01	0.36
Model 2[e] (restricted)		−0.45			0.04		0.15
F-test (p)[f]							0.01
Frontal_Mid_Orb							
Model 1[d] (full)	−0.70	−1.02	−1.75	0.05	0.02	0.05	0.45
Model 2[e] (restricted)		−0.43			0.05		0.17
F-test (p)[f]							0.002
Supp_Motor_Area							
Model 1[d] (full)	−1.39	−1.84	−2.47	0.03	0.03	0.03	0.37
Model 2[e] (restricted)		−0.38			0.04		0.15
F-test (p)[f]							0.01
Hippocampus							
Model 1[d] (full)	−3.52	−0.71	−4.78	0.01	0.05	0.01	0.35
Model 2[e] (restricted)		−0.29			0.05		0.15
F-test (p)[f]							0.05
Lingual							
Model 1[d] (full)	−2.76	−1.19	−2.96	0.05	0.03	0.05	0.33
Model 2[e] (restricted)		−0.37			0.04		0.15
F-test (p)[f]							0.03

Key: Aβ, β-amyloid; CBVa, CBVa, arteriolar cerebral blood volume; GM, gray matter.
[a] The brain regions were labeled according to the IBASPM 116 atlas (please see Methods for references).
[b] The estimated coefficients correspond to β1, β2, and β3 in Equation for CBVa, Aβ, and CBVa × Aβ, respectively. The synergistic effect from CBVa and Aβ is reflected in the β3 term.
[c] The standardized coefficient can be used as an estimate of relative contribution to longitudinal cognitive decline from each term.
[d] Model 1: cognitive decline (% per year) = β0 + β1 × CBVa + β2 × Aβ + β3 × CBVa × Aβ + β4 × sex + β5 × age + β6 × education.
[e] Model 2: cognitive decline (% per year) = β0 + β2 × Aβ + β4 × sex + β5 × age + β6 × education.
[f] p-Value from R² change F-test to assess whether the R² from the 2 models are significantly different.

previously by measuring the transverse (T2) relaxation time of the iVASO difference signal, which is highly sensitive to the blood oxygenation level (Hua et al., 2011b). Given the importance of capillaries for tissue perfusion in healthy brain and in AD and MCI (Eskildsen et al., 2017; Nielsen et al., 2017a), future studies should also investigate potential abnormalities in capillaries in MCI using specialized methods.

One fundamental limitation of this pilot study is the time difference between the PET imaging and the MRI scans. To assess long-term effects of Aβ, in the present study, 7T MRI was administered approximately 2 years after the initial 11C-PiB-PET. Considering the gradual accumulation of Aβ in AD, which takes almost 2 decades before the threshold-level of pathological Aβ characterizing the clinical syndrome is reached (Dubois et al., 2016; Roberts et al., 2017), the chosen temporal delay of 2 years should allow for detecting long-term effects of Aβ on CBVa, while still remaining within the AD predemedia phase. However, as currently not much is known on possible determinants of Aβ dynamics in clinical populations, our findings of a relationship between local Aβ and CBVa might be affected by possibly existing differences in cerebral Aβ accumulation between study participants. In this regard, our preliminary results should be interpreted with caution, and both PET and MRI will be administrated at the initial and the follow-up visits in subsequent studies to validate the current findings. In addition, as our assessment of individual cognitive decline per year does not account for practice effects or regression to the mean, effects associated with cognition need to be interpreted with caution and replicated by prospective longitudinal studies.

Another important limitation of the study is that all variables, including APOE4 status, were treated as linear in the multiple regression analysis. While such linear mixed models are commonly adopted in similar studies (Mormino et al., 2014), they may not reflect accurate relationship between cognitive decline and these variables. More detailed modeling is merited in subsequent studies to explore and describe more precise relationships between these measures.

Finally, it is possible that PET SUVr may show correlation with CBF simply because the PET tracer reaches its target via the blood flow. However, as we assessed the steady state effect with cortical late-frames for estimating SUVr, that is, 50−70 minutes after 11C-PiB injection, influence from the dynamic relationship between 11C PiB SUVr and CBF at earlier TPs should be negligible. Indeed, it has been shown that 11C-PiB retention did not correlate with regional CBF (Chen et al., 2015). Moreover, according to the central volume theorem, CBF = CBVa/arterial transit time (ATT), such dynamic interaction between CBF and PET SUVr should primarily be driven by changes in ATT. In iVASO, heterogeneity of ATT is accounted for with data acquired at multiple TIs and the fitting algorithm in the iVASO theory (Hua et al., 2011c). Therefore, the correlation between CBVa and PET SUVr observed in our data should be minimally affected by the potential interaction between CBF and PET SUVr. Although in our data only regional interactions between 11C-PiB SUVr and CBVa were observable, the possibility of a general confounding effect on quantification of the iVASO signal should nevertheless be considered. In addition, potential interindividual differences in the susceptibility to Aβ burden might be a

Table 6
Multilevel regression analysis on the synergistic effects from GM CBVa and β-amyloid on cognitive decline using data from the control and MCI subjects as 2 separate groups

Region[a]	Standardized coefficient[b,c]			p-Value			R²
	CBVa (β1)	Aβ (β2)	CBVa × Aβ (β3)	CBVa (β1)	Aβ (β2)	CBVa × Aβ (β3)	
Frontal_Sup_Orb							
Model 1[d] (full)	−1.40	−0.58	−1.85	0.05	0.05	0.04	0.32
Model 2[e] (restricted)		−0.25			0.05		0.16
F-test (p)[f]							0.05
Frontal_Inf_Orb							
Model 1[d] (full)	−1.40	−0.95	−1.85	0.05	0.03	0.05	0.39
Model 2[e] (restricted)		−0.57			0.05		0.15
F-test (p)[f]							0.01
Frontal_Sup_Medial							
Model 1[d] (full)	−1.46	−0.95	−2.22	0.02	0.02	0.01	0.32
Model 2[e] (restricted)		−0.46			0.03		0.17
F-test (p)[f]							0.02
Frontal_Mid_Orb							
Model 1[d] (full)	−0.66	−0.99	−1.84	0.04	0.02	0.04	0.41
Model 2[e] (restricted)		−0.44			0.04		0.16
F-test (p)[f]							0.005
Supp_Motor_Area							
Model 1[d] (full)	−1.38	−1.82	−2.52	0.03	0.03	0.03	0.37
Model 2[e] (restricted)		−0.46			0.04		0.15
F-test (p)[f]							0.01
Hippocampus							
Model 1[d] (full)	−3.46	−0.67	−4.85	0.01	0.04	0.01	0.37
Model 2[e] (restricted)		−0.25			0.05		0.15
F-test (p)[f]							0.04
Lingual							
Model 1[d] (full)	−2.72	−1.15	−3.03	0.04	0.03	0.04	0.32
Model 2[e] (restricted)		−0.42			0.04		0.16
F-test (p)[f]							0.05

[a] The brain regions were labeled according to the IBASPM 116 atlas (please see Methods for references).
[b] The estimated coefficients correspond to β1, β2, and β3 in Equation for CBVa, Aβ, and CBVa × Aβ, respectively. The synergistic effect from CBVa and Aβ is reflected in the β3 term.
[c] The standardized coefficient can be used as an estimate of relative contribution to longitudinal cognitive decline from each term.
[d] Model 1: Cognitive decline (% per year) = β0+ β1 × CBVa+ β2 × Aβ+ β3 × CBVa × Aβ+ β4 × sex + β5 × age + β6 × education+ β7 × age × Aβ.
[e] Model 2: Cognitive decline (% per year) = β0+ β2 × Aβ+ β4 × sex + β5 × age + β6 × education.
[f] p-Value from R² change F-test to assess whether the R² from the 2 models are significantly different.

confounding factor (van Bergen et al., 2018a). Furthermore, because of the highly specialized experimental setup including both 7T MRI and 11C-PiB, which needed to be performed in the vicinity of the cyclotron used for manufacturing the tracer, a multi-center approach was not feasible, resulting in a relatively small sample size. However, while the application of ultrahigh field strength MRI for maximizing SNR may have increased power to detect early Aβ-related CBVa changes, future larger studies are needed to reproduce our findings in a more clinical setting.

5. Conclusion

Taken together, we here provide evidence on increases in CBVa that are observable in older adults with MCI and closely relate to local Aβ, APOE4, and cognitive decline within 2 years. Although our data support earlier considerations on a close relationship between AD pathology and neurovascular dysfunction, additional research is needed to investigate whether elevated CBVa in the predementia stage of AD may represent a marker of secondary vascular pathology associated with Aβ accumulation and thus resulting damage to the neurovascular unit. Alternatively, increased CBVa in the pre-dementia stage may represent a compensatory mechanism aimed at maintaining stable cerebral perfusion and oxygen supply despite spreading AD pathology.

Disclosure

Equipment used in the study was manufactured by Philips. Dr. van Zijl is a paid lecturer for Philips Healthcare and has technology licensed to Philips Healthcare. This arrangement has been approved by Johns Hopkins University in accordance with its conflict of interest policies. All other authors declare that they have no conflict of interest.

Acknowledgements

and acquisition of PiB-PET data. VT and AB supervised the preparation of the 11C PiB tracer for measuring brain Aβ-plaque density, quality control of PET data and analysis, revision of the article. RMN and CH are the chairmen of the department and sponsors of the study and provided critical revisions of the final article. HL provided critical revisions of the final article. PCMVZ provided critical revisions of the final article. MA provided critical revisions of the final article. PGU designed the study and experimental setup, supervised the acquisition, processing, analysis, and interpretation of neuroimaging as well as clinical data. PGU has drafted the article together with JH; PGU has performed the final revision and is corresponding author.

Appendix A. Supplementary data

Supplementary data associated with this article can be found, in the online version, at https://doi.org/10.1016/j.neurobiolaging.2019.01.001.

References

Aaslid, R., Lindegaard, K.F., Sorteberg, W., Nornes, H., 1989. Cerebral autoregulation dynamics in humans. Stroke 20, 45—52.

Albert, M.S., DeKosky, S.T., Dickson, D., Dubois, B., Feldman, H.H., Fox, N.C., Gamst, A., Holtzman, D.M., Jagust, W.J., Petersen, R.C., Snyder, P.J., Carrillo, M.C., Thies, B., Phelps, C.H., 2011. The diagnosis of mild cognitive impairment due to Alzheimer's disease: recommendations from the National Institute on Aging-Alzheimer's Association workgroups on diagnostic guidelines for Alzheimer's disease. Alzheimers Dement. : J. Alzheimers Assoc. 7, 270—279.

Alsop, D.C., Dai, W., Grossman, M., Detre, J.A., 2010. Arterial spin labeling blood flow MRI: its role in the early characterization of Alzheimer's disease. J. Alzheimers Dis. 20, 871—880.

Bell, R.D., Zlokovic, B.V., 2009. Neurovascular mechanisms and blood-brain barrier disorder in Alzheimer's disease. Acta Neuropathol. 118, 103—113.

Benjamini, Y., Hochberg, Y., 1995. Controlling the false discovery rate: a practical and powerful approach to multiple testing. J. R. Stat. Soc. Series B Methodol. 57, 289—300.

Bennett, R.E., Robbins, A.B., Hu, M., Cao, X., Betensky, R.A., Clark, T., Das, S., Hyman, B.T., 2018. Tau induces blood vessel abnormalities and angiogenesis-related gene expression in P301L transgenic mice and human Alzheimer's disease. Proc. Natl. Acad. Sci. U. S. A. 115, E1289—E1298.

Brickman, A.M., Guzman, V.A., Gonzalez-Castellon, M., Razlighi, Q., Gu, Y., Narkhede, A., Janicki, S., Ichise, M., Stern, Y., Manly, J.J., Schupf, N., Marshall, R.S., 2015. Cerebral autoregulation, beta amyloid, and white matter hyperintensities are interrelated. Neurosci. Lett. 592, 54—58.

Chen, Y.J., Rosario, B.L., Mowrey, W., Laymon, C.M., Lu, X., Lopez, O.L., Klunk, W.E., Lopresti, B.J., Mathis, C.A., Price, J.C., 2015. Relative 11C-PiB delivery as a proxy of relative CBF: quantitative evaluation using single-session 15O-water and 11C-PiB PET. J. Nucl. Med. 56, 1199—1205.

Corder, E.H., Saunders, A.M., Strittmatter, W.J., Schmechel, D.E., Gaskell, P.C., Small, G.W., Roses, A.D., Haines, J.L., Pericak-Vance, M.A., 1993. Gene dose of apolipoprotein E type 4 allele and the risk of Alzheimer's disease in late onset families. Science 261, 921—923.

Donahue, M.J., Sideso, E., MacIntosh, B.J., Kennedy, J., Handa, A., Jezzard, P., 2010. Absolute arterial cerebral blood volume quantification using inflow vascular-space-occupancy with dynamic subtraction magnetic resonance imaging. J. Cereb. Blood Flow Metab. 30, 1329—1342.

Dubois, B., Hampel, H., Feldman, H.H., Scheltens, P., Aisen, P., Andrieu, S., Bakardjian, H., Benali, H., Bertram, L., Blennow, K., Broich, K., Cavedo, E., Crutch, S., Dartigues, J.F., Duyckaerts, C., Epelbaum, S., Frisoni, G.B., Gauthier, S., Genthon, R., Gouw, A.A., Habert, M.O., Holtzman, D.M., Kivipelto, M., Lista, S., Molinuevo, J.L., O'Bryant, S.E., Rabinovici, G.D., Rowe, C., Salloway, S., Schneider, L.S., Sperling, R., Teichmann, M., Carrillo, M.C., Cummings, J., Jack Jr., C.R., Proceedings of the Meeting of the International Working, Group, the American Alzheimer's Association on "The Preclinical State of, A.D.", July, Washington DC, USA, 2016. Preclinical Alzheimer's disease: Definition, natural history, and diagnostic criteria. Alzheimers Dement. : J. Alzheimers Assoc. 12, 292—323.

Dvorak, H.F., Nagy, J.A., Feng, D., Brown, L.F., Dvorak, A.M., 1999. Vascular permeability factor/vascular endothelial growth factor and the significance of microvascular hyperpermeability in angiogenesis. Curr. Top. Microbiol. Immunol. 237, 97—132.

Elahi, F.M., Miller, B.L., 2017. A clinicopathological approach to the diagnosis of dementia. Nat. Rev. Neurol. 13, 457—476.

Eskildsen, S.F., Gyldensted, L., Nagenthiraja, K., Nielsen, R.B., Hansen, M.B., Dalby, R.B., Frandsen, J., Rodell, A., Gyldensted, C., Jespersen, S.N., Lund, T.E., Mouridsen, K., Braendgaard, H., Ostergaard, L., 2017. Increased cortical capillary

transit time heterogeneity in Alzheimer's disease: a DSC-MRI perfusion study. Neurobiol. Aging 50, 107—118.

Folstein, M.F., Folstein, S.E., McHugh, P.R., 1975. "Mini-mental state". A practical method for grading the cognitive state of patients for the clinician. J. Psychiatr. Res. 12, 189—198.

Gelber, R.P., Launer, L.J., White, L.R., 2012. The Honolulu-Asia Aging Study: epidemiologic and neuropathologic research on cognitive impairment. Curr. Alzheimer Res. 9, 664—672.

Gietl, A.F., Warnock, G., Riese, F., Kalin, A.M., Saake, A., Gruber, E., Leh, S.E., Unschuld, P.G., Kuhn, F.P., Burger, C., Mu, L., Seifert, B., Nitsch, R.M., Schibli, R., Ametamey, S.M., Buck, A., Hock, C., 2015. Regional cerebral blood flow estimated by early PiB uptake is reduced in mild cognitive impairment and associated with age in an amyloid-dependent manner. Neurobiol. Aging 36, 1619—1628.

Gregoire, J., Van der Linden, M., 1997. Effect of age on forward and backward digit spans. Aging Neuropsychol. Cogn. 4, 140—149.

Gröhn, O.H., Lukkarinen, J.A., Oja, J.M., van Zijl, P.C., Ulatowski, J.A., Traystman, R.J., Kauppinen, R.A., 1998. Noninvasive detection of cerebral hypoperfusion and reversible ischemia from reductions in the magnetic resonance imaging relaxation time, T2. J. Cereb. Blood Flow Metab. 18, 911—920.

Grubb Jr., R.L., Raichle, M.E., Eichling, J.O., Ter-Pogossian, M.M., 1974. The effects of changes in PaCO2 on cerebral blood volume, blood flow, and vascular mean transit time. Stroke 5, 630—639.

Harada, C.N., Natelson Love, M.C., Triebel, K.L., 2013. Normal cognitive aging. Clin. Geriatr. Med. 29, 737—752.

Harris, G.J., Lewis, R.F., Satlin, A., English, C.D., Scott, T.M., Yurgelun-Todd, D.A., Renshaw, P.F., 1996. Dynamic susceptibility contrast MRI of regional cerebral blood volume in Alzheimer's disease. Am. J. Psychiatry 153, 721—724.

Hauser, T., Schonknecht, P., Thomann, P.A., Gerigk, L., Schroder, J., Henze, R., Radbruch, A., Essig, M., 2013. Regional cerebral perfusion alterations in patients with mild cognitive impairment and Alzheimer disease using dynamic susceptibility contrast MRI. Acad. Radiol. 20, 705—711.

Helzner, E.P., Luchsinger, J.A., Scarmeas, N., Cosentino, S., Brickman, A.M., Glymour, M.M., Stern, Y., 2009. Contribution of vascular risk factors to the progression in Alzheimer disease. Arch. Neurol. 66, 343—348.

Hirao, K., Ohnishi, T., Hirata, Y., Yamashita, F., Mori, T., Moriguchi, Y., Matsuda, H., Nemoto, K., Imabayashi, E., Yamada, M., Iwamoto, T., Arima, K., Asada, T., 2005. The prediction of rapid conversion to Alzheimer's disease in mild cognitive impairment using regional cerebral blood flow SPECT. Neuroimage 28, 1014—1021.

Hua, J., Brandt, A.S., Lee, S., Blair, N.I.S., Wu, Y., Lui, S., Patel, J., Faria, A.V., Lim, I.A.L., Unschuld, P.G., Pekar, J.J., van Zijl, P.C.M., Ross, C.A., Margolis, R.L., 2017. Abnormal grey matter arteriolar cerebral blood volume in schizophrenia measured with 3D inflow-based vascular-space-occupancy MRI at 7T. Schizophr. Bull. 43, 620—632.

Hua, J., Jones, C.K., Qin, Q., van Zijl, P.C., 2013. Implementation of vascular-space-occupancy MRI at 7T. Magn. Reson. Med. 69, 1003—1013.

Hua, J., Lee, S., Blair, N.I.S., Brandt, A., Patel, J., Faria, A.V., Lim, I.A., Pekar, J.J., van Zijl, P.C.M., Ross, C.A., Margolis, R.L., 2015. Reduced Grey Matter Arteriolar Cerebral Blood Volume in Schizophrenia. Proc 23rd Annual Meeting ISMRM, Toronto, Canada.

Hua, J., Liu, P., Kim, T., Donahue, M., Rane, S., Chen, J.J., Qin, Q., Kim, S.G., 2018. MRI techniques to measure arterial and venous cerebral blood volume. Neuroimage. https://doi.org/10.1016/j.neuroimage.2018.02.027.

Hua, J., Qin, Q., Donahue, M.J., Zhou, J., Pekar, J.J., van Zijl, P.C., 2011a. Inflow-based vascular-space-occupancy (iVASO) MRI. Magn. Reson. Med. 66, 40—56.

Hua, J., Qin, Q., Pekar, J.J., Zijl, P.C., 2011b. Measurement of absolute arterial cerebral blood volume in human brain without using a contrast agent. NMR Biomed. 24, 1313—1325.

Hua, J., Qin, Q., Pekar, J.J., Zijl, P.C., 2011c. Measurement of absolute arterial cerebral blood volume in human brain without using a contrast agent. NMR Biomed. 24, 1313—1325.

Hua, J., Unschuld, P.G., Margolis, R.L., van Zijl, P.C., Ross, C.A., 2014. Elevated arteriolar cerebral blood volume in prodromal Huntington's disease. Mov. Disord. 29, 396—401.

Iadecola, C., 2003. Cerebrovascular effects of amyloid-beta peptides: mechanisms and implications for Alzheimer's dementia. Cell. Mol. Neurobiol. 23, 681—689.

Iadecola, C., 2004. Neurovascular regulation in the normal brain and in Alzheimer's disease. Nat. Rev. Neurosci. 5, 347—360.

Iadecola, C., Nedergaard, M., 2007. Glial regulation of the cerebral microvasculature. Nat. Neurosci. 10, 1369—1376.

Iliff, J.J., Lee, H., Yu, M., Feng, T., Logan, J., Nedergaard, M., Benveniste, H., 2013. Brain-wide pathway for waste clearance captured by contrast-enhanced MRI. J. Clin. Invest. 123, 1299—1309.

Iliff, J.J., Wang, M., Liao, Y., Plogg, B.A., Peng, W., Gundersen, G.A., Benveniste, H., Vates, G.E., Deane, R., Goldman, S.A., Nagelhus, E.A., Nedergaard, M., 2012. A paravascular pathway facilitates CSF flow through the brain parenchyma and the clearance of interstitial solutes, including amyloid beta. Sci. Transl. Med. 4, 147ra11.

Ito, H., Ibaraki, M., Kanno, I., Fukuda, H., Miura, S., 2005. Changes in the arterial fraction of human cerebral blood volume during hypercapnia and hypocapnia measured by positron emission tomography. J. Cereb. Blood Flow Metab. 25, 852—857.

Ito, H., Kanno, I., Iida, H., Hatazawa, J., Shimosegawa, E., Tamura, H., Okudera, T., 2001. Arterial fraction of cerebral blood volume in humans measured by positron emission tomography. Ann. Nucl. Med. 15, 111—116.

Iturria-Medina, Y., Sotero, R.C., Toussaint, P.J., Mateos-Perez, J.M., Evans, A.C., Alzheimer's Disease Neuroimaging, I., 2016. Early role of vascular dysregulation on

late-onset Alzheimer's disease based on multifactorial data-driven analysis. Nat. Commun. 7, 11934.

Jack Jr., C.R., Knopman, D.S., Jagust, W.J., Shaw, L.M., Aisen, P.S., Weiner, M.W., Petersen, R.C., Trojanowski, J.Q., 2010. Hypothetical model of dynamic biomarkers of the Alzheimer's pathological cascade. Lancet Neurol. 9, 119—128.

Janelidze, S., Hertze, J., Nagga, K., Nilsson, K., Nilsson, C., , Swedish Bio, F.S.G., Wennstrom, M., van Westen, D., Blennow, K., Zetterberg, H., Hansson, O., 2017. Increased blood-brain barrier permeability is associated with dementia and diabetes but not amyloid pathology or APOE genotype. Neurobiol. Aging 51, 104—112.

Jansen, W.J., Ossenkoppele, R., Knol, D.L., Tijms, B.M., Scheltens, P., Verhey, F.R., Visser, P.J., , Amyloid Biomarker Study, G., Aalten, P., Aarsland, D., Alcolea, D., Alexander, M., Almdahl, I.S., Arnold, S.E., Baldeiras, I., Barthel, H., van Berckel, B.N., Bibeau, K., Blennow, K., Brooks, D.J., van Buchem, M.A., Camus, V., Cavedo, E., Chen, K., Chetelat, G., Cohen, A.D., Drzezga, A., Engelborghs, S., Fagan, A.M., Fladby, T., Fleisher, A.S., van der Flier, W.M., Ford, L., Forster, S., Fortea, J., Foskett, N., Frederiksen, K.S., Freund-Levi, Y., Frisoni, G.B., Froelich, L., Gabryelewicz, T., Gill, K.D., Gkatzima, O., Gomez-Tortosa, E., Gordon, M.F., Grimmer, T., Hampel, H., Hausner, L., Hellwig, S., Herukka, S.K., Hildebrandt, H., Ishihara, L., Ivanoiu, A., Jagust, W.J., Johannsen, P., Kandimalla, R., Kapaki, E., Klimkowicz-Mrowiec, A., Klunk, W.E., Kohler, S., Koglin, N., Kornhuber, J., Kramberger, M.G., Van Laere, K., Landau, S.M., Lee, D.Y., de Leon, M., Lisetti, V., Lleo, A., Madsen, K., Maier, W., Marcusson, J., Mattsson, N., de Mendonca, A., Meulenbroek, O., Meyer, P.T., Mintun, M.A., Mok, V., Molinuevo, J.L., Mollergard, H.M., Morris, J.C., Mroczko, B., Van der Mussele, S., Na, D.L., Newberg, A., Nordberg, A., Nordlund, A., Novak, G.P., Paraskevas, G.P., Parnetti, L., Perera, G., Peters, O., Popp, J., Prabhakar, S., Rabinovici, G.D., Ramakers, I.H., Rami, L., Resende de Oliveira, C., Rinne, J.O., Rodrigue, K.M., Rodriguez-Rodriguez, E., Roe, C.M., Rot, U., Rowe, C.C., Ruther, E., Sabri, O., Sanchez-Juan, P., Santana, I., Sarazin, M., Schroder, J., Schutte, C., Seo, S.W., Soetewey, F., Soininen, H., Spiru, L., Struyfs, H., Teunissen, C.E., Tsolaki, M., Vandenberghe, R., Verbeek, M.M., Villemagne, V.L., Vos, S.J., van Waalwijk van Doorn, L.J., Waldemar, G., Wallin, A., Wallin, A.K., Wiltfang, J., Wolk, D.A., Zboch, M., Zetterberg, H., 2015. Prevalence of cerebral amyloid pathology in persons without dementia: a meta-analysis. JAMA 313, 1924—1938.

Johnson, N.A., Jahng, G.H., Weiner, M.W., Miller, B.L., Chui, H.C., Jagust, W.J., Gorno-Tempini, M.L., Schuff, N., 2005. Pattern of cerebral hypoperfusion in Alzheimer disease and mild cognitive impairment measured with arterial spin-labeling MR imaging: initial experience. Radiology 234, 851—859.

Kantarci, K., Lowe, V., Przybelski, S.A., Weigand, S.D., Senjem, M.L., Ivnik, R.J., Preboske, G.M., Roberts, R., Geda, Y.E., Boeve, B.F., Knopman, D.S., Petersen, R.C., Jack Jr., C.R., 2012. APOE modifies the association between Abeta load and cognition in cognitively normal older adults. Neurology 78, 232—240.

Kim, T., Hendrich, K.S., Masamoto, K., Kim, S.G., 2007. Arterial versus total blood volume changes during neural activity-induced cerebral blood flow change: implication for BOLD fMRI. J. Cereb. Blood Flow Metab. 27, 1235—1247.

Kisler, K., Nelson, A.R., Montagne, A., Zlokovic, B.V., 2017. Cerebral blood flow regulation and neurovascular dysfunction in Alzheimer disease. Nat. Rev. Neurosci. 18, 419—434.

Klunk, W.E., Engler, H., Nordberg, A., Wang, Y., Blomqvist, G., Holt, D.P., Bergstrom, M., Savitcheva, I., Huang, G.F., Estrada, S., Ausen, B., Debnath, M.L., Barletta, J., Price, J.C., Sandell, J., Lopresti, B.J., Wall, A., Koivisto, P., Antoni, G., Mathis, C.A., Langstrom, B., 2004. Imaging brain amyloid in Alzheimer's disease with Pittsburgh compound-B. Ann. Neurol. 55, 306—319.

Kreczmanski, P., Heinsen, H., Mantua, V., Woltersdorf, F., Masson, T., Ulfig, N., Schmidt-Kastner, R., Korr, H., Steinbusch, H.W., Hof, P.R., Schmitz, C., 2009. Microvessel length density, total length, and length per neuron in five subcortical regions in schizophrenia. Acta Neuropathol. 117, 409—421.

Kreczmanski, P., Schmidt-Kastner, R., Heinsen, H., Steinbusch, H.W., Hof, P.R., Schmitz, C., 2005. Stereological studies of capillary length density in the frontal cortex of schizophrenics. Acta Neuropathol. 109, 510—518.

Lacalle-Aurioles, M., Mateos-Perez, J.M., Guzman-De-Villoria, J.A., Olazaran, J., Cruz-Orduna, I., Aleman-Gomez, Y., Martino, M.E., Desco, M., 2014. Cerebral blood flow is an earlier indicator of perfusion abnormalities than cerebral blood volume in Alzheimer's disease. J. Cereb. Blood Flow Metab. 34, 654—659.

Lancaster, J.L., Rainey, L.H., Summerlin, J.L., Freitas, C.S., Fox, P.T., Evans, A.C., Toga, A.W., Mazziotta, J.C., 1997. Automated labeling of the human brain: a preliminary report on the development and evaluation of a forward-transform method. Hum. Brain Mapp. 5, 238—242.

Lancaster, J.L., Woldorff, M.G., Parsons, L.M., Liotti, M., Freitas, C.S., Rainey, L., Kochunov, P.V., Nickerson, D., Mikiten, S.A., Fox, P.T., 2000. Automated talairach atlas labels for functional brain mapping. Hum. Brain Mapp. 10, 120—131.

Lange, K.L., Bondi, M.W., Salmon, D.P., Galasko, D., Delis, D.C., Thomas, R.G., Thal, L.J., 2002. Decline in verbal memory during preclinical Alzheimer's disease: examination of the effect of APOE genotype. J. Int. Neuropsychol. Soc. 8, 943—955.

Leeuwis, A.E., Benedictus, M.R., Kuijer, J.P.A., Binnewijzend, M.A.A., Hooghiemstra, A.M., Verfaillie, S.C.J., Koene, T., Scheltens, P., Barkhof, F., Prins, N.D., van der Flier, W.M., 2017. Lower cerebral blood flow is associated with impairment in multiple cognitive domains in Alzheimer's disease. Alzheimers Dement. : J. Alzheimers Assoc. 13, 531—540.

Lu, H., Donahue, M.J., van Zijl, P.C., 2006. Detrimental effects of BOLD signal in arterial spin labeling fMRI at high field strength. Magn. Reson. Med. 56, 546—552.

Maldjian, J.A., Laurienti, P.J., Burdette, J.H., 2004. Precentral gyrus discrepancy in electronic versions of the Talairach atlas. Neuroimage 21, 450—455.

Maldjian, J.A., Laurienti, P.J., Kraft, R.A., Burdette, J.H., 2003. An automated method for neuroanatomic and cytoarchitectonic atlas-based interrogation of fMRI data sets. Neuroimage 19, 1233—1239.

Marques, J.P., Kober, T., Krueger, G., van der Zwaag, W., Van de Moortele, P.F., Gruetter, R., 2010. MP2RAGE, a self bias-field corrected sequence for improved segmentation and T1-mapping at high field. Neuroimage 49, 1271—1281.

Mawuenyega, K.G., Sigurdson, W., Ovod, V., Munsell, L., Kasten, T., Morris, J.C., Yarasheski, K.E., Bateman, R.J., 2010. Decreased clearance of CNS beta-amyloid in Alzheimer's disease. Science 330, 1774.

Michels, L., Warnock, G., Buck, A., Macauda, G., Leh, S.E., Kaelin, A.M., Riese, F., Meyer, R., O'Gorman, R., Hock, C., Kollias, S., Gietl, A.F., 2016. Arterial spin labeling imaging reveals widespread and Abeta-independent reductions in cerebral blood flow in elderly apolipoprotein epsilon-4 carriers. J. Cereb. Blood Flow Metab. 36, 581—595.

Mishra, A., 2016. Angiogenic neovessels promote tissue hypoxia. Proc. Natl. Acad. Sci. U. S. A. 113, 10458—10460.

Mormino, E.C., Betensky, R.A., Hedden, T., Schultz, A.P., Amariglio, R.E., Rentz, D.M., Johnson, K.A., Sperling, R.A., 2014. Synergistic effect of beta-amyloid and neurodegeneration on cognitive decline in clinically normal individuals. JAMA Neurol. 71, 1379—1385.

Mormino, E.C., Kluth, J.T., Madison, C.M., Rabinovici, G.D., Baker, S.L., Miller, B.L., Koeppe, R.A., Mathis, C.A., Weiner, M.W., Jagust, W.J., Alzheimer's Disease Neuroimaging, I., 2009. Episodic memory loss is related to hippocampal-mediated beta-amyloid deposition in elderly subjects. Brain 132 (Pt 5), 1310—1323.

Murray, M.E., Lowe, V.J., Graff-Radford, N.R., Liesinger, A.M., Cannon, A., Przybelski, S.A., Rawal, B., Parisi, J.E., Petersen, R.C., Kantarci, K., Ross, O.A., Duara, R., Knopman, D.S., Jack Jr., C.R., Dickson, D.W., 2015. Clinicopathologic and 11C-Pittsburgh compound B implications of Thal amyloid phase across the Alzheimer's disease spectrum. Brain 138 (Pt 5), 1370—1381.

Nicholas, L.E., Brookshire, R.H., D.L, M., Schumacher, J.G., Porrazzo, S.A., 1988. The Boston naming test: revised administration and scoring procedures and normative information for non-brain-damaged adults. Clin. Aphasiology 18, 103—115.

Nielsen, R.B., Egefjord, L., Angleys, H., Mouridsen, K., Gejl, M., Moller, A., Brock, B., Braendgaard, H., Gottrup, H., Rungby, J., Eskildsen, S.F., Ostergaard, L., 2017a. Capillary dysfunction is associated with symptom severity and neurodegeneration in Alzheimer's disease. Alzheimers Dement. : J. Alzheimers Assoc. 13, 1143—1153.

Nielsen, R.B., Egefjord, L., Angleys, H., Mouridsen, K., Gejl, M., Moller, A., Brock, B., Braendgaard, H., Gottrup, H., Rungby, J., Eskildsen, S.F., Ostergaard, L., 2017b. Capillary dysfunction is associated with symptom severity and neurodegeneration in Alzheimer's disease. Alzheimers Dement. : J. Alzheimers Assoc. 13, 1143—1153.

Niwa, K., Porter, V.A., Kazama, K., Cornfield, D., Carlson, G.A., Iadecola, C., 2001. A beta-peptides enhance vasoconstriction in cerebral circulation. Am. J. Physiol. Heart Circ. Physiol. 281, H2417—H2424.

Ossenkoppele, R., Jansen, W.J., Rabinovici, G.D., Knol, D.L., van der Flier, W.M., van Berckel, B.N., Scheltens, P., Visser, P.J., , Amyloid, P.E.T.S.G., Verfaillie, S.C., Zwan, M.D., Adriaanse, S.M., Lammertsma, A.A., Barkhof, F., Jagust, W.J., Miller, B.L., Rosen, H.J., Landau, S.M., Villemagne, V.L., Rowe, C.C., Lee, D.Y., Na, D.L., Seo, S.W., Sarazin, M., Roe, C.M., Sabri, O., Barthel, H., Koglin, N., Hodges, J., Leyton, C.E., Vandenberghe, R., van Laere, K., Drzezga, A., Forster, S., Grimmer, T., Sanchez-Juan, P., Carril, J.M., Mok, V., Camus, V., Klunk, W.E., Cohen, A.D., Meyer, P.T., Hellwig, S., Newberg, A., Frederiksen, K.S., Fleisher, A.S., Mintun, M.A., Wolk, D.A., Nordberg, A., Rinne, J.O., Chetelat, G., Lleo, A., Blesa, R., Fortea, J., Madsen, K., Rodrigue, K.M., Brooks, D.J., 2015. Prevalence of amyloid PET positivity in dementia syndromes: a meta-analysis. JAMA 313, 1939—1949.

Ostergaard, L., Aamand, R., Gutierrez-Jimenez, E., Ho, Y.C., Blicher, J.U., Madsen, S.M., Nagenthiraja, K., Dalby, R.B., Drasbek, K.R., Moller, A., Braendgaard, H., Mouridsen, K., Jespersen, S.N., Jensen, M.S., West, M.J., 2013. The capillary dysfunction hypothesis of Alzheimer's disease. Neurobiol. Aging 34, 1018—1031.

Pappolla, M.A., Bryant-Thomas, T.K., Herbert, D., Pacheco, J., Fabra Garcia, M., Manjon, M., Girones, X., Henry, T.L., Matsubara, E., Zambon, D., Wolozin, B., Sano, M., Cruz-Sanchez, F.F., Thal, L.J., Petanceska, S.S., Refolo, L.M., 2003. Mild hypercholesterolemia is an early risk factor for the development of Alzheimer amyloid pathology. Neurology 61, 199—205.

Petrella, J.R., Provenzale, J.M., 2000. MR perfusion imaging of the brain: techniques and applications. AJR Am. J. Roentgenol. 175, 207—219.

Piechnik, S.K., Chiarelli, P.A., Jezzard, P., 2008. Modelling vascular reactivity to investigate the basis of the relationship between cerebral blood volume and flow under CO2 manipulation. Neuroimage 39, 107—118.

Puro, D.G., Kohmoto, R., Fujita, Y., Gardner, T.W., Padovani-Claudio, D.A., 2016. Bioelectric impact of pathological angiogenesis on vascular function. Proc. Natl. Acad. Sci. U. S. A. 113, 9934—9939.

Quevenco, F.C., Preti, M.G., van Bergen, J., Hua, J., Wyss, M., Li, X., Schreiner, S.J., Steininger, S.C., Meyer, R., Meier, I.B., Brickman, A.M., Leh, S.E., Gietl, A.F., Buck, A., Nitsch, R.M., Pruessmann, K.P., van Zijl, P.C., Hock, C., Van De Ville, D., Unschuld, P.G., 2017. Memory performance-related dynamic brain connectivity indicates pathological burden and genetic risk for Alzheimer's disease. Alzheimers Res. Ther. 9, 24.

Rabinovici, G.D., Carrillo, M.C., Forman, M., DeSanti, S., Miller, D.S., Kozauer, N., Petersen, R.C., Randolph, C., Knopman, D.S., Smith, E.E., Isaac, M., Mattsson, N., Bain, L.J., Hendrix, J.A., Sims, J.R., 2017. Multiple comorbid neuropathologies in

the setting of Alzheimer's disease neuropathology and implications for drug development. Alzheimers Dement. (N. Y.) 3, 83–91.

Rane, S., Talati, P., Donahue, M.J., Heckers, S., 2016. Inflow-vascular space occupancy (iVASO) reproducibility in the hippocampus and cortex at different blood water nulling times. Magn. Reson. Med. 75, 2379–2387.

Roberts, B.R., Lind, M., Wagen, A.Z., Rembach, A., Frugier, T., Li, Q.X., Ryan, T.M., McLean, C.A., Doecke, J.D., Rowe, C.C., Villemagne, V.L., Masters, C.L., 2017. Biochemically-defined pools of amyloid-beta in sporadic Alzheimer's disease: correlation with amyloid PET. Brain 140, 1486–1498.

Roher, A.E., Garami, Z., Tyas, S.L., Maarouf, C.L., Kokjohn, T.A., Belohlavek, M., Vedders, L.J., Connor, D., Sabbagh, M.N., Beach, T.G., Emmerling, M.R., 2011. Transcranial Doppler ultrasound blood flow velocity and pulsatility index as systemic indicators for Alzheimer's disease. Alzheimers Dement. : J. Alzheimers Assoc. 7, 445–455.

Ruitenberg, A., den Heijer, T., Bakker, S.L., van Swieten, J.C., Koudstaal, P.J., Hofman, A., Breteler, M.M., 2005. Cerebral hypoperfusion and clinical onset of dementia: the Rotterdam Study. Ann. Neurol. 57, 789–794.

Schreiner, S.J., Kirchner, T., Narkhede, A., Wyss, M., Van Bergen, J.M.G., Steininger, S.C., Gietl, A., Leh, S.E., Treyer, V., Buck, A., Pruessmann, K.P., Nitsch, R.M., Hock, C., Henning, A., Brickman, A.M., Unschuld, P.G., 2018. Brain amyloid burden and cerebrovascular disease are synergistically associated with neurometabolism in cognitively unimpaired older adults. Neurobiol. Aging 63, 152–161.

Schreiner, S.J., Kirchner, T., Wyss, M., Van Bergen, J.M., Quevenco, F.C., Steininger, S.C., Griffith, E.Y., Meier, I., Michels, L., Gietl, A.F., Leh, S.E., Brickman, A.M., Hock, C., Nitsch, R.M., Pruessmann, K.P., Henning, A., Unschuld, P.G., 2016. Low episodic memory performance in cognitively normal elderly subjects is associated with increased posterior cingulate gray matter N-acetylaspartate: a 1H MRSI study at 7 Tesla. Neurobiol. Aging 48, 195–203.

Schreiner, S.J., Liu, X., Gietl, A.F., Wyss, M., Steininger, S.C., Gruber, E., Treyer, V., Meier, I.B., Kalin, A.M., Leh, S.E., Buck, A., Nitsch, R.M., Pruessmann, K.P., Hock, C., Unschuld, P.G., 2014. Regional fluid-attenuated inversion recovery (FLAIR) at 7 Tesla correlates with amyloid beta in hippocampus and brainstem of cognitively normal elderly subjects. Front Aging Neurosci. 6, 240.

Seo, S.W., Ayakta, N., Grinberg, L.T., Villeneuve, S., Lehmann, M., Reed, B., DeCarli, C., Miller, B.L., Rosen, H.J., Boxer, A.L., O'Neil, J.P., Jin, L.W., Seeley, W.W., Jagust, W.J., Rabinovici, G.D., 2017. Regional correlations between [(11)C]PIB PET and post-mortem burden of amyloid-beta pathology in a diverse neuropathological cohort. Neuroimage Clin. 13, 130–137.

Serrano-Pozo, A., Frosch, M.P., Masliah, E., Hyman, B.T., 2011. Neuropathological alterations in Alzheimer disease. Cold Spring Harb. Perspect. Med. 1, a006189.

Sharan, M., Jones Jr., M.D., Koehler, R.C., Traystman, R.J., Popel, A.S., 1989. A compartmental model for oxygen transport in brain microcirculation. Ann. Biomed. Eng. 17, 13–38.

Smith, S.M., Nichols, T.E., 2009. Threshold-free cluster enhancement: addressing problems of smoothing, threshold dependence and localisation in cluster inference. Neuroimage 44, 83–98.

Snowdon, D.A., Nun, S., 2003. Healthy aging and dementia: findings from the Nun Study. Ann. Intern. Med. 139 (5 Pt 2), 450–454.

Steininger, S.C., Liu, X., Gietl, A., Wyss, M., Schreiner, S., Gruber, E., Treyer, V., Kalin, A., Leh, S., Buck, A., Nitsch, R.M., Prussmann, K.P., Hock, C., Unschuld, P.G., 2014. Cortical amyloid beta in cognitively normal elderly adults is associated with decreased network efficiency within the cerebro-cerebellar system. Front Aging Neurosci. 6, 52.

Strittmatter, W.J., Saunders, A.M., Schmechel, D., Pericak-Vance, M., Enghild, J., Salvesen, G.S., Roses, A.D., 1993. Apolipoprotein E: high-avidity binding to beta-amyloid and increased frequency of type 4 allele in late-onset familial Alzheimer disease. Proc. Natl. Acad. Sci. U. S. A. 90, 1977–1981.

Suri, S., Mackay, C.E., Kelly, M.E., Germuska, M., Tunbridge, E.M., Frisoni, G.B., Matthews, P.M., Ebmeier, K.P., Bulte, D.P., Filippini, N., 2015. Reduced cerebrovascular reactivity in young adults carrying the APOE epsilon4 allele. Alzheimers Dement. : J. Alzheimers Assoc. 11, 648–657.e1.

Takano, T., Tian, G.F., Peng, W., Lou, N., Libionka, W., Han, X., Nedergaard, M., 2006. Astrocyte-mediated control of cerebral blood flow. Nat. Neurosci. 9, 260–267.

Thambisetty, M., Beason-Held, L., An, Y., Kraut, M.A., Resnick, S.M., 2010. APOE epsilon4 genotype and longitudinal changes in cerebral blood flow in normal aging. Arch. Neurol. 67, 93–98.

Thomas, T., Miners, S., Love, S., 2015. Post-mortem assessment of hypoperfusion of cerebral cortex in Alzheimer's disease and vascular dementia. Brain 138 (Pt 4), 1059–1069.

Thore, C.R., Anstrom, J.A., Moody, D.M., Challa, V.R., Marion, M.C., Brown, W.R., 2007. Morphometric analysis of arteriolar tortuosity in human cerebral white matter of preterm, young, and aged subjects. J. Neuropathol. Exp. Neurol. 66, 337–345.

Tombaugh, T.N., 2004. Trail making test A and B: normative data stratified by age and education. Arch. Clin. Neuropsychol. 19, 203–214.

Tyas, S.L., Salazar, J.C., Snowdon, D.A., Desrosiers, M.F., Riley, K.P., Mendiondo, M.S., Kryscio, R.J., 2007a. Transitions to mild cognitive impairments, dementia, and death: findings from the Nun Study. Am. J. Epidemiol. 165, 1231–1238.

Tyas, S.L., Snowdon, D.A., Desrosiers, M.F., Riley, K.P., Markesbery, W.R., 2007b. Healthy ageing in the Nun Study: definition and neuropathologic correlates. Age Ageing 36, 650–655.

Tzourio-Mazoyer, N., Landeau, B., Papathanassiou, D., Crivello, F., Etard, O., Delcroix, N., Mazoyer, B., Joliot, M., 2002. Automated anatomical labeling of activations in SPM using a macroscopic anatomical parcellation of the MNI MRI single-subject brain. Neuroimage 15, 273–289.

Uh, J., Lewis-Amezcua, K., Martin-Cook, K., Cheng, Y., Weiner, M., Diaz-Arrastia, R., Devous Sr., M., Shen, D., Lu, H., 2010. Cerebral blood volume in Alzheimer's disease and correlation with tissue structural integrity. Neurobiol. Aging 31, 2038–2046.

Uranova, N.A., Zimina, I.S., Vikhreva, O.V., Krukov, N.O., Rachmanova, V.I., Orlovskaya, D.D., 2010. Ultrastructural damage of capillaries in the neocortex in schizophrenia. World J. Biol. Psychiatry : Off. J. World Fed. Soc. Biol. Psychiatry 11, 567–578.

van Bergen, J.M., Li, X., Hua, J., Schreiner, S.J., Steininger, S.C., Quevenco, F.C., Wyss, M., Gietl, A.F., Treyer, V., Leh, S.E., Buck, F., Nitsch, R.M., Pruessmann, K.P., van Zijl, P.C., Hock, C., Unschuld, P.G., 2016. Colocalization of cerebral iron with amyloid beta in mild cognitive impairment. Sci. Rep. 6, 35514.

van Bergen, J.M.G., Li, X., Quevenco, F.C., Gietl, A.F., Treyer, V., Leh, S.E., Meyer, R., Buck, A., Kaufmann, P.A., Nitsch, R.M., van Zijl, P.C.M., Hock, C., Unschuld, P.G., 2018a. Low cortical iron and high entorhinal cortex volume promote cognitive functioning in the oldest-old. Neurobiol. Aging 64, 68–75.

van Bergen, J.M.G., Li, X., Quevenco, F.C., Gietl, A.F., Treyer, V., Meyer, R., Buck, A., Kaufmann, P.A., Nitsch, R.M., van Zijl, P.C.M., Hock, C., Unschuld, P.G., 2018b. Simultaneous quantitative susceptibility mapping and Flutemetamol-PET suggests local correlation of iron and beta-amyloid as an indicator of cognitive performance at high age. Neuroimage 174, 308–316.

Van de Moortele, P.F., Auerbach, E.J., Olman, C., Yacoub, E., Ugurbil, K., Moeller, S., 2009. T1 weighted brain images at 7 Tesla unbiased for Proton Density, T2* contrast and RF coil receive B1 sensitivity with simultaneous vessel visualization. Neuroimage 46, 432–446.

van Zijl, P.C., Eleff, S.M., Ulatowski, J.A., Oja, J.M., Ulug, A.M., Traystman, R.J., Kauppinen, R.A., 1998. Quantitative assessment of blood flow, blood volume and blood oxygenation effects in functional magnetic resonance imaging. Nat. Med. 4, 159–167.

Verghese, P.B., Castellano, J.M., Garai, K., Wang, Y., Jiang, H., Shah, A., Bu, G., Frieden, C., Holtzman, D.M., 2013. ApoE influences amyloid-beta (Abeta) clearance despite minimal apoE/Abeta association in physiological conditions. Proc. Natl. Acad. Sci. U. S. A. 110, E1807–E1816.

Villemagne, V.L., Dore, V., Burnham, S.C., Masters, C.L., Rowe, C.C., 2018. Imaging tau and amyloid-beta proteinopathies in Alzheimer disease and other conditions. Nat. Rev. Neurol. 14, 225–236.

Wirth, M., Bejanin, A., La Joie, R., Arenaza-Urquijo, E.M., Gonneaud, J., Landeau, B., Perrotin, A., Mezenge, F., de La Sayette, V., Desgranges, B., Chetelat, G., 2017. Regional patterns of gray matter volume, hypometabolism, and beta-amyloid in groups at risk of Alzheimer's disease. Neurobiol. Aging 63, 140–151.

World_Medical_Association, 1991. Declaration of Helsinki. Law Med. Health Care 19, 264–265.

Wu, Y., Agarwal, S., Jones, C.K., Webb, A.G., van Zijl, P.C., Hua, J., Pillai, J.J., 2016. Measurement of arteriolar blood volume in brain tumors using MRI without exogenous contrast agent administration at 7T. J. Magn. Reson. Imaging 44, 1244–1255.

Xie, L., Kang, H., Xu, Q., Chen, M.J., Liao, Y., Thiyagarajan, M., O'Donnell, J., Christensen, D.J., Nicholson, C., Iliff, J.J., Takano, T., Deane, R., Nedergaard, M., 2013. Sleep drives metabolite clearance from the adult brain. Science 342, 373–377.

Yoshiura, T., Hiwatashi, A., Yamashita, K., Ohyagi, Y., Monji, A., Takayama, Y., Nagao, E., Kamano, H., Noguchi, T., Honda, H., 2009. Simultaneous measurement of arterial transit time, arterial blood volume, and cerebral blood flow using arterial spin-labeling in patients with Alzheimer disease. AJNR Am. J. Neuroradiol. 30, 1388–1393.

Zlokovic, B.V., 2011. Neurovascular pathways to neurodegeneration in Alzheimer's disease and other disorders. Nat. Rev. Neurosci. 12, 723–738.